AD-A160 965 LOCALIZED ELF PROPAGATION ANOMALIES(U) PACIFIC-SIERRA RESEARCH CORP LOS ANGELES CA E C FIELD ET AL JUN 85 PSR-1441 N00014-84-C-0214 1/1

UNCLASSIFIED F/G 20/14 NL

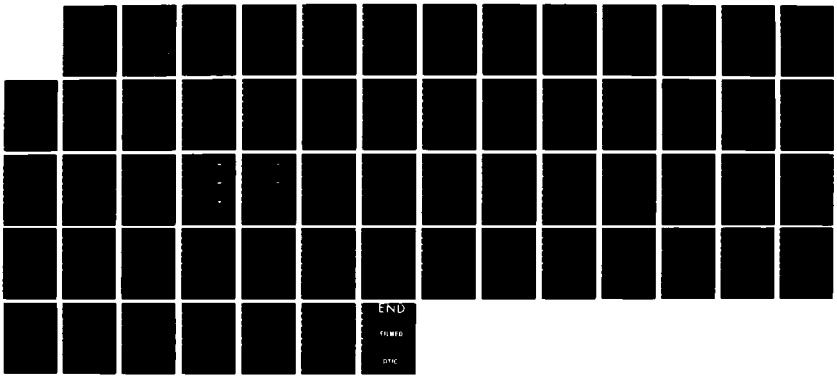

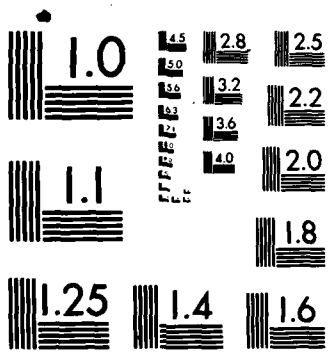

MICROCOPY RESOLUTION TEST CHART
NATIONAL BUREAU OF STANDARDS-1963-A

(12)

AD-A160 965

PSR Report 1441

LOCALIZED ELF PROPAGATION ANOMALIES

E. C. Field, Jr.
C. R. Warber

June 1985

Final Technical Report
Contract N00014-84-C-0214

Sponsored by
Office of Naval Research
800 North Quincy Street
Arlington, Virginia 22217

DTIC
ELECTE
NOV 0 7 1985
S D
E

DTIC FILE COPY

PACIFIC-SIERRA RESEARCH CORP.
12340 Santa Monica Blvd. • Los Angeles, CA 90025 • (213) 820-2200

85 11 07 001

PSR Report 1441

LOCALIZED ELF PROPAGATION ANOMALIES

E. C. Field, Jr.
C. R. Warber

June 1985

Accession For
NTIS GRA&I ☒
DTIC TAB ☐
Unannounced ☐
Justification
By
Distribution/
Availability Codes
Dist | Avail and/or Special
A-1

Final Technical Report
Contract N00014-84-C-0214

Sponsored by
Office of Naval Research
800 North Quincy Street
Arlington, Virginia 22217

QUALITY INSPECTED 3

PACIFIC-SIERRA RESEARCH CORP.
12340 Santa Monica Blvd. • Los Angeles, CA 90025 • (213) 820-2200

This document has been approved for public release and sale; its distribution is unlimited.

UNCLASSIFIED

SECURITY CLASSIFICATION OF THIS PAGE

AD-A160965

REPORT DOCUMENTATION PAGE

1a. REPORT SECURITY CLASSIFICATION UNCLASSIFIED	1b. RESTRICTIVE MARKINGS
2a. SECURITY CLASSIFICATION AUTHORITY	3. DISTRIBUTION/AVAILABILITY OF REPORT
2b. DECLASSIFICATION/DOWNGRADING SCHEDULE	Unclassified/Unlimited
4. PERFORMING ORGANIZATION REPORT NUMBER(S) PSR Report 1441	5. MONITORING ORGANIZATION REPORT NUMBER(S)
6a. NAME OF PERFORMING ORGANIZATION Pacific-Sierra Research Corporation 6b. OFFICE SYMBOL (If applicable)	7a. NAME OF MONITORING ORGANIZATION
6c. ADDRESS (City, State, and ZIP Code) 12340 Santa Monica Boulevard Los Angeles, California 90025	7b. ADDRESS (City, State, and ZIP Code)
8a. NAME OF FUNDING/SPONSORING ORGANIZATION Office of Naval Research 8b. OFFICE SYMBOL (If applicable) Code 414	9. PROCUREMENT INSTRUMENT IDENTIFICATION NUMBER N00014-84-C-0214
8c. ADDRESS (City, State, and ZIP Code) 800 North Quincy Street Arlington, Virginia 22217	10. SOURCE OF FUNDING NUMBERS PROGRAM ELEMENT NO. 61153N; PROJECT NO. 021-01-02; TASK NO. NR089-172; WORK UNIT ACCESSION NO.

11. TITLE (Include Security Classification)
LOCALIZED ELF PROPAGATION ANOMALIES

12. PERSONAL AUTHOR(S)
E. C. Field, Jr., C. R. Warber

13a. TYPE OF REPORT	13b. TIME COVERED	14. DATE OF REPORT (Year, Month, Day)	15. PAGE COUNT
Draft Final Technical	FROM March 84 TO Dec 84	1984 December	

16. SUPPLEMENTARY NOTATION

17. COSATI CODES			18. SUBJECT TERMS (Continue on reverse if necessary and identify by block number)
FIELD	GROUP	SUB-GROUP	Extremely-low-frequency propagation Low-frequency propagation Polar cap absorption event Solar proton event Submarine communications

19. ABSTRACT (Continue on reverse if necessary and identify by block number)

Two methods are used to analyze ELF propagation near lateral nonhomogeneities in the earth-ionosphere waveguide. The first, a full-wave integral equation, is accurate but expensive to solve, and the second, a two-dimensional ray trace, is only semiquantitative but provides physical insight. Both methods are applied to several model SPEs, including one based on the 23 November 1982 event, which is of special interest because simultaneous measurements of ELF signal anomalies and incident proton fluxes are available. Calculations predict a region of weak field near the Gulf of Alaska, where a submarine-borne receiver measured an unusually severe signal loss. That behavior is caused by lateral refraction, which bends the signal away from the gulf and into the disturbed polar cap, where the phase velocity of the TEM mode is lowest. The theory also predicts a region of strong field just inside the polar cap boudary, but no data are available to test that

20. DISTRIBUTION/AVAILABILITY OF ABSTRACT ☐ UNCLASSIFIED/UNLIMITED ☒ SAME AS RPT ☐ DTIC USERS	21. ABSTRACT SECURITY CLASSIFICATION Unclassified
22a. NAME OF RESPONSIBLE INDIVIDUAL	22b. TELEPHONE (Include Area Code) / 22c. OFFICE SYMBOL

DD FORM 1473, 84 MAR — 83 APR edition may be used until exhausted. All other editions are obsolete.

SECURITY CLASSIFICATION OF THIS PAGE
UNCLASSIFIED

19. ABSTRACT (Continued)

result. Localized regions of weak or strong fields will occur on links where the great-circle path is nearly tangent to a boundary between large zones with different ionospheric or ground properties and hence, different waveguide phase velocities.

SUMMARY

Two methods are used to analyze extremely low frequency (ELF) propagation near lateral nonhomogeneities in the earth-ionosphere waveguide. The first, a full-wave integral equation, is accurate although expensive to solve and the second, a two-dimensional ray trace, is only semiquantitative but provides physical insight. Both methods are applied to several model solar proton events (SPEs), including one based on the 23 November 1982 event, which is of special interest because simultaneous measurements of ELF signal anomalies and incident proton fluxes are available. Calculations predict a region of weak field near the Gulf of Alaska, where a submarine-borne receiver measured an unusually severe signal loss. That behavior is caused by lateral refraction, which bends the signal away from the gulf and into the disturbed polar cap, where the phase velocity of the TEM mode is lowest. The theory also predicts a region of strong field just inside the polar cap boundary, but no data are available to test that result. Localized regions of weak or strong fields will occur on links where the great-circle path is nearly tangent to a boundary between large zones with different ionospheric or ground properties and hence, different waveguide phase velocities.

CONTENTS

SUMMARY iii

FIGURES vii

TABLES ix

Section

I. INTRODUCTION 1

II. ELF ANOMALIES MEASURED DURING SOLAR PROTON EVENTS 4

III. ELECTRON AND ION DENSITY PROFILES UNDER POLAR CAP 8

IV. PROPAGATION MODEL OF NOVEMBER 1982 SPE 12
Propagation in Stratified Waveguide 12
Calculated Propagation Parameters 13
Polar Cap Boundary Model 15

V. TWO-DIMENSIONAL RAY TRACE: LATERAL REFRACTION OF TEM MODE 19

VI. FULL-WAVE CALCULATIONS USING INTEGRAL WAVE EQUATION 26
Integral Wave Equation 26
Numerical Results 28

VII. CONCLUSIONS 32

Appendix

A. CALCULATION OF IONIZATION PROFILES FROM PROTON FLUXES .. 33

B. RAY TRACING IN TWO DIMENSIONS 39

REFERENCES 51

FIGURES

1. Geometry of propagation path from WTF to Gulf of Alaska 5

2. Signal received in Gulf of Alaska: 23 November 1982 6

3. Integral proton fluxes averaged over geomagnetic latitudes greater than 70 deg (NOA66 satellite measurement) 9

4. Electron and ion densities at 0800 UT: 23 November 1982 10

5. Electron and ion densities at 1600 UT: 23 November 1982 11

6. Integral proton fluxes versus geomagnetic latitude: 8 December 1982 16

7. Model of polar cap propagation constant 17

8. Schematic of propagation model 18

9. Ray tracing for SPEs of various strengths 22

10. Ray tracing for weak SPE and various transition zone widths 24

11. Contour plot of $|W|$ in dB//1 for weak SPE, $S_{SPE} = 1.25$ (transition zone width = 0.5 Mm) 29

12. Contour plot of $|W|$ in dB//1 for weak SPE, $S_{SPE} = 1.25$ (transition zone width = 1 Mm) 30

13. Contour plot of $|W|$ in dB//1 for strong SPE, $S_{SPE} = 1.45$ (transition zone width = 1 Mm) 31

A.1. Strength and rigidity parameters: 23 November 1982 34

A.2. Ionization per proton of given energy 35

A.3. Electron and ion collision frequencies 38

B.1. Validity condition for $S_{SPE} = 1.25$ 50

TABLES

1. Calculated propagation parameters at 76 Hz 14

A.1. Energy bands used to find ion-pair production rates 36

B.1. Validity criterion for three examples 49

I. INTRODUCTION

Extremely low frequency (ELF) signals radiated from the Wisconsin Test Facility (WTF) often exhibit anomalies that are too strong and localized to be caused by global changes in the attenuation rate, which is low. Moreover, those anomalies could not be caused by mode interference, because, at ELF, only the TEM mode can propagate. A satisfactory explanation requires a theory that accommodates lateral inhomogeneities in the earth-ionosphere waveguide.

It is not surprising that waveguide nonstratification must be accounted for at ELF. Even such large inhomogeneities as sporadic-E patches, the disturbed polar cap, and the day/night terminator can cause the properties of the earth-ionosphere waveguide to change markedly over the huge wavelength or Fresnel zone of an ELF signal. At higher frequencies, the wavelength or Fresnel zone is usually much smaller than the scale lengths of lateral variations in the waveguide.

Field and Joiner [1979, 1982] derived an integral equation that describes ELF fields when the earth-ionosphere waveguide is not stratified. Since no directly applicable propagation data were available at that time, they applied the theory to hypothetical ionospheric disturbances, to nominal models of the day/night terminator, and to the disturbed polar cap. Their results show that strong localized anomalies could be caused by focussing, diffraction, and reflection of the TEM mode.

Pappert [1980] used an integral formulation to analyze the effects of sporadic-E patches on ELF propagation. It was found that at night, such patches could cause severe fades. The physical mechanism is resonant attenuation that occurs when the vertical wavelength of the ELF wave matches the optical thickness of the sporadic-E layer. Because of the masking effect of the D-region, that resonant attenuation would not be seen in the daytime.

Bannister [1982] summarizes nocturnal ELF anomalies measured simultaneously in the northeastern U.S. and on board submarines in the

North Atlantic. The northeastern U.S. signals faded by many decibels in a few hours although the propagation paths were only about 1.6 Mm long. In the North Atlantic, three submarines separated by less than 2 Mm measured signals that differed from one another by up to 7 dB. Some of those anomalies had forms similar to ones measured in the northeastern U.S. a few hours earlier. Moreover, they exhibited amplitude and phase fluctuations consistent with those predicted by Pappert [1980]. Therefore, they were likely caused by nocturnal sporadic-E patches drifting from west to east. A number of anomalies were observed in the northeastern U.S., but no simultaneous measurements were made at other sites. Although sporadic-E patches could have caused those anomalies, an alternative explanation is standing-wave or diffraction patterns caused by the interaction of the TEM mode with the polar cap boundary.

Katan and Bannister [forthcoming] also report several anomalies measured by the Naval Underwater Systems Center (NUSC) at a number of locations during the solar proton events (SPEs) of 13 February 1978, 22 to 26 November 1982, and 8 December 1982. The measurements of the WTF signal made in Connecticut and on board submarines in the Gulf of Alaska and the North Atlantic are the most relevant to this report. In those cases anomalies were observed, although the great-circle propagation path passed near, but not beneath, the disturbed polar cap. During the weak 23 November 1982 SPE a submarine in the Gulf of Alaska measured a fade deeper than that occurring on longer paths that passed through the main portion of the disturbed polar cap during much stronger events. That behavior cannot be explained with the often used WKB treatment of ELF propagation which attributes all propagation phenomena to the state of the ionosphere directly over the great-circle path.

This report treats as a test case, the anomalies measured in the Gulf of Alaska during the 22 to 26 November 1982 SPE. It compares the results obtained using two computational methods: (1) a full-wave integral equation solution, and (2) a two-dimensional ray trace that accounts for lateral refraction of the TEM mode in the nonstratified earth-ionosphere waveguide.

The NOAA6 and GOES2 satellites measured incident proton fluxes as a function of time and latitude during the above three SPEs. Those important auxiliary data are used as inputs to air-chemistry codes to calculate the electron and ion density height-profiles at the time of the ELF anomalies. Those profiles are, in turn, used as inputs to our propagation calculations. Thus, the measured and calculated ELF fields can be compared under disturbed conditions using actual, rather than nominal, ionospheric profiles.

II. ELF ANOMALIES MEASURED DURING SOLAR PROTON EVENTS

Measurements of ELF amplitude and phase were made by Katan and Bannister [forthcoming] during several SPEs that occurred between the years 1976 and 1982. Some of the measurements were made on land, and others were made on board submarines whose locations cannot be specified precisely. However, the receiver locations are known well enough for the present analysis.

The strengths of the SPEs during the time ELF measurements were made varied widely--the strongest on 13 February 1978 caused 8 dB of riometer absorption and the weakest on 23 November 1982 caused only 0.8 dB riometer absorption. Care must be used in interpreting those strengths because riometer absorption and ELF propagation are governed by different regions of the ionosphere. It is not unusual for larger ELF effects to be observed during a weak SPE than during a strong one.

This report concentrates on a weak SPE that occurred on 23 November 1982, and caused propagation effects greater than can be explained in terms of propagation in a nearly stratified earth-ionosphere waveguide. On 23 November 1982 the WTF transmitted a signal that was received on board a submarine in the Gulf of Alaska. The approximate geometry of the great-circle propagation path, the disturbed polar cap, and the first Fresnel zone at a frequency of 76 Hz are given in Fig. 1. Note that the great-circle propagation path is nearly tangent to the edge of the polar cap, which covers about one-half the Fresnel zone.

The signal received in the Gulf of Alaska on 23 November 1982 is plotted in Fig. 2. Also plotted in Fig. 2 is an average ambient signal for that location. The amplitude of the disturbed signal was 3 to 4 dB below the ambient signal during the night, and about 2 dB below the ambient signal during the day. This behavior occurred because the incident proton flux had diminished considerably by sunrise on 23 November. The relative phase of the signal remained close to its ambient value throughout the measurement period.

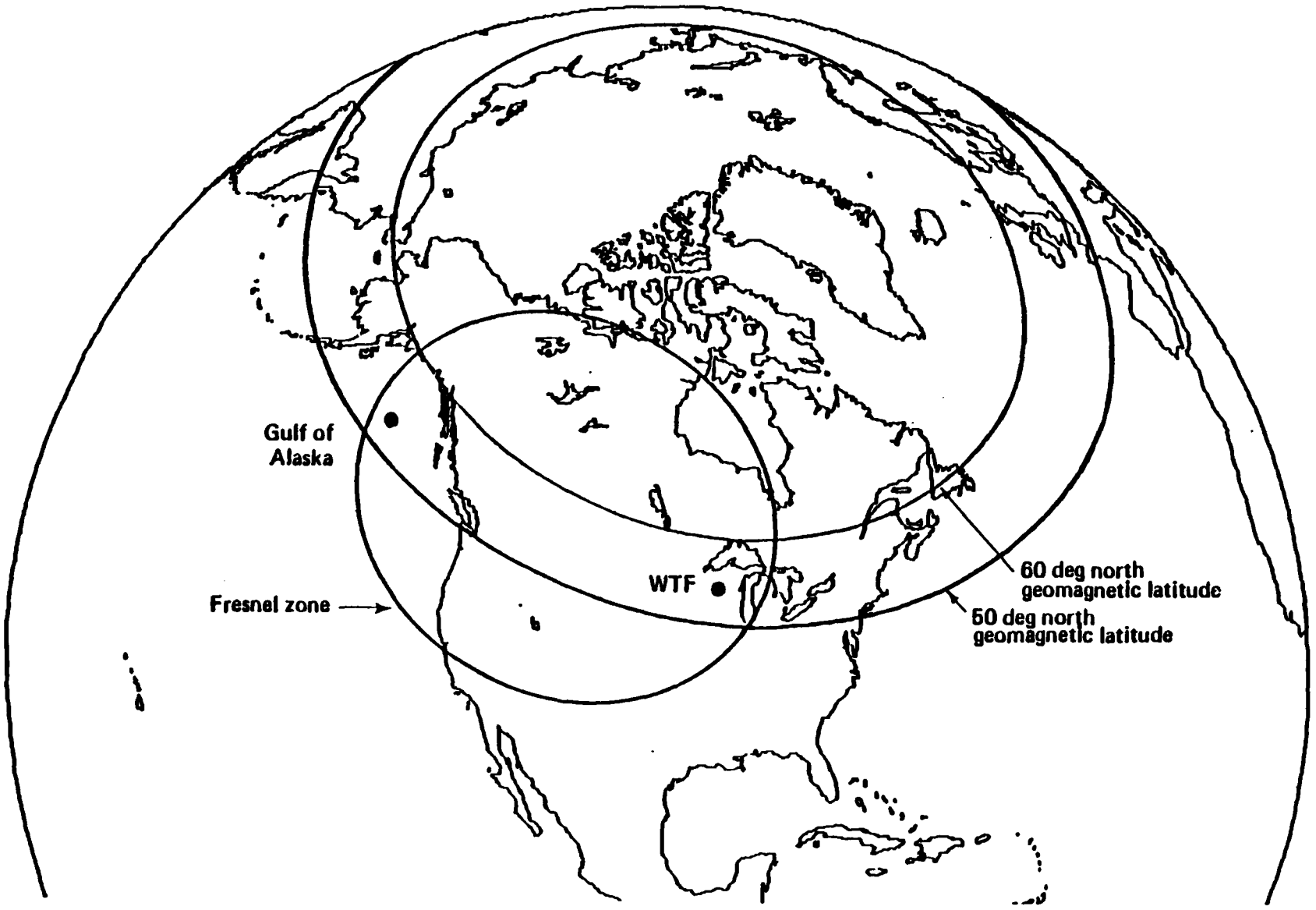

Fig. 1--Geometry of propagation path from WTF to Gulf of Alaska

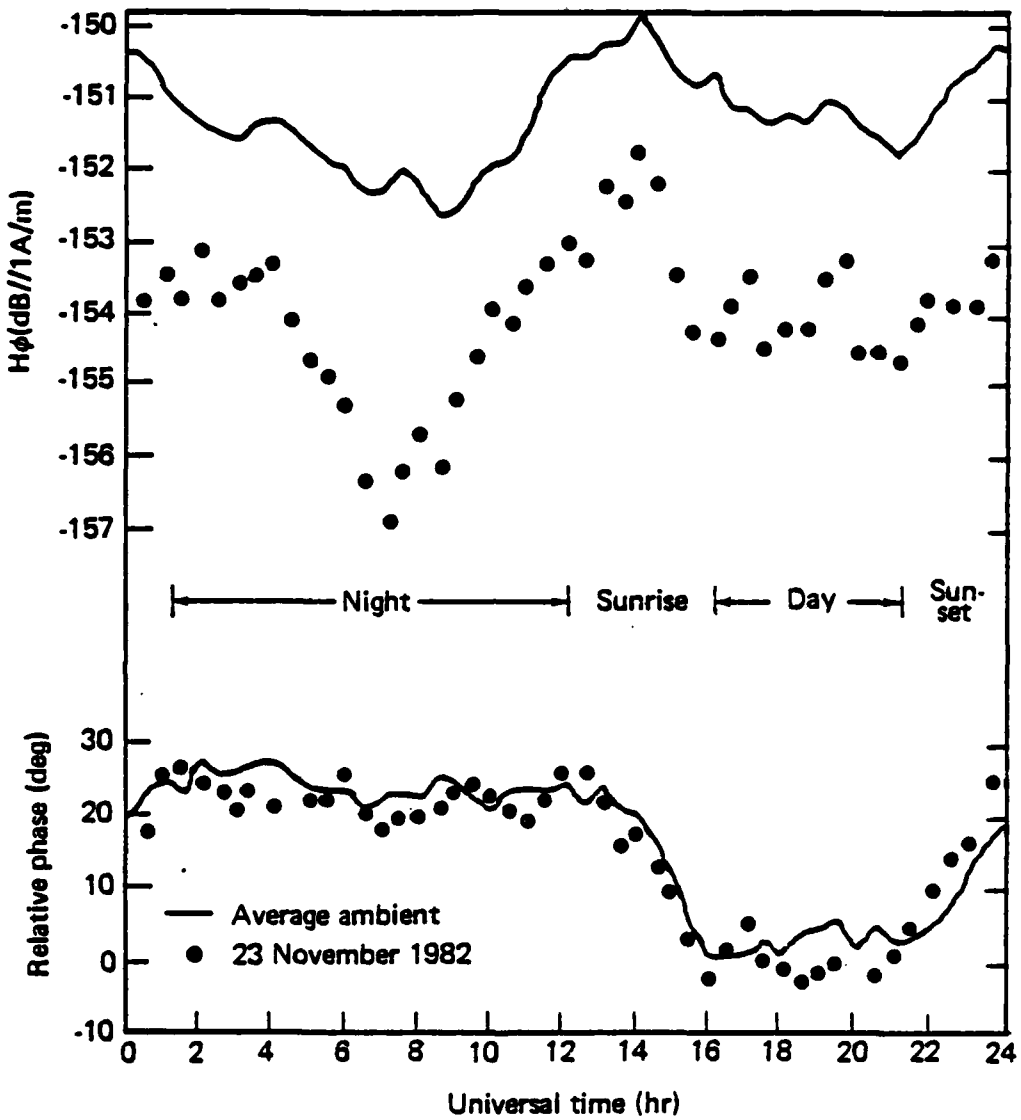

Fig. 2--Signal received in Gulf of Alaska:
23 November 1982

The large magnitude of the SPE-induced signal loss revealed in Fig. 2 is surprising given the following three factors: (1) the weakness of the 23 November SPE, (2) the relative shortness of the propagation path (3.5 Mm), and (3) the great-circle path having missed the main portion of the disturbed polar cap. For comparison, we note that smaller signal losses were caused by the stronger 8 December 1982 SPE (2 dB riometer absorption) on longer paths that traversed the center of the polar cap [Katan and Bannister, forthcoming]. The explanation lies in the propagation geometry given in Fig. 1, which causes lateral refraction and reflection and, thus, shadow zones and interference patterns [Field and Joiner, 1982].

III. ELECTRON AND ION DENSITY PROFILES UNDER POLAR CAP

The NOAA6 low-altitude polar-orbiting satellite measured integral proton fluxes in four channels defined by E > 2.5, 16, 36, and 80 Mev, where E is the proton energy. Those data are shown in Fig. 3, for the end of 1982 November [Sauer, 1983]. The event began at approximately 1600 UT on 23 November and lasted at least until the middle of 24 November. A second and larger SPE commenced on 26 November. The fluxes plotted in Fig. 3 are averaged over magnetic latitudes higher than 70 deg. The proton flux deviates only slightly from its spatial average, provided the latitude exceeds 60 deg. Therefore, the fluxes given in Fig. 3 represent those throughout the main portion of the disturbed polar cap.

The proton fluxes are used to calculate the energy deposition and the profiles of ion-pair production rates in the ionosphere during the SPE. These production rates are inserted into the lumped-parameter ionization-balance equations, which are solved numerically for the electron and ion density profiles. This calculation of particle densities is described in Appendix A.

The calculated electron and ion densities at 0800 UT on 23 November (which is local night in the Gulf of Alaska) are presented in Fig. 4. The profiles calculated between 0200 and 1100 UT differed only slightly from those shown in Fig. 4 and are not included here. In Fig. 5, profiles calculated at 1800 UT (which is local daytime in the Gulf of Alaska) are presented. Only small variations were found among profiles calculated at different daylight hours. For comparison, Figs. 4 and 5 plot nominal ambient profiles.

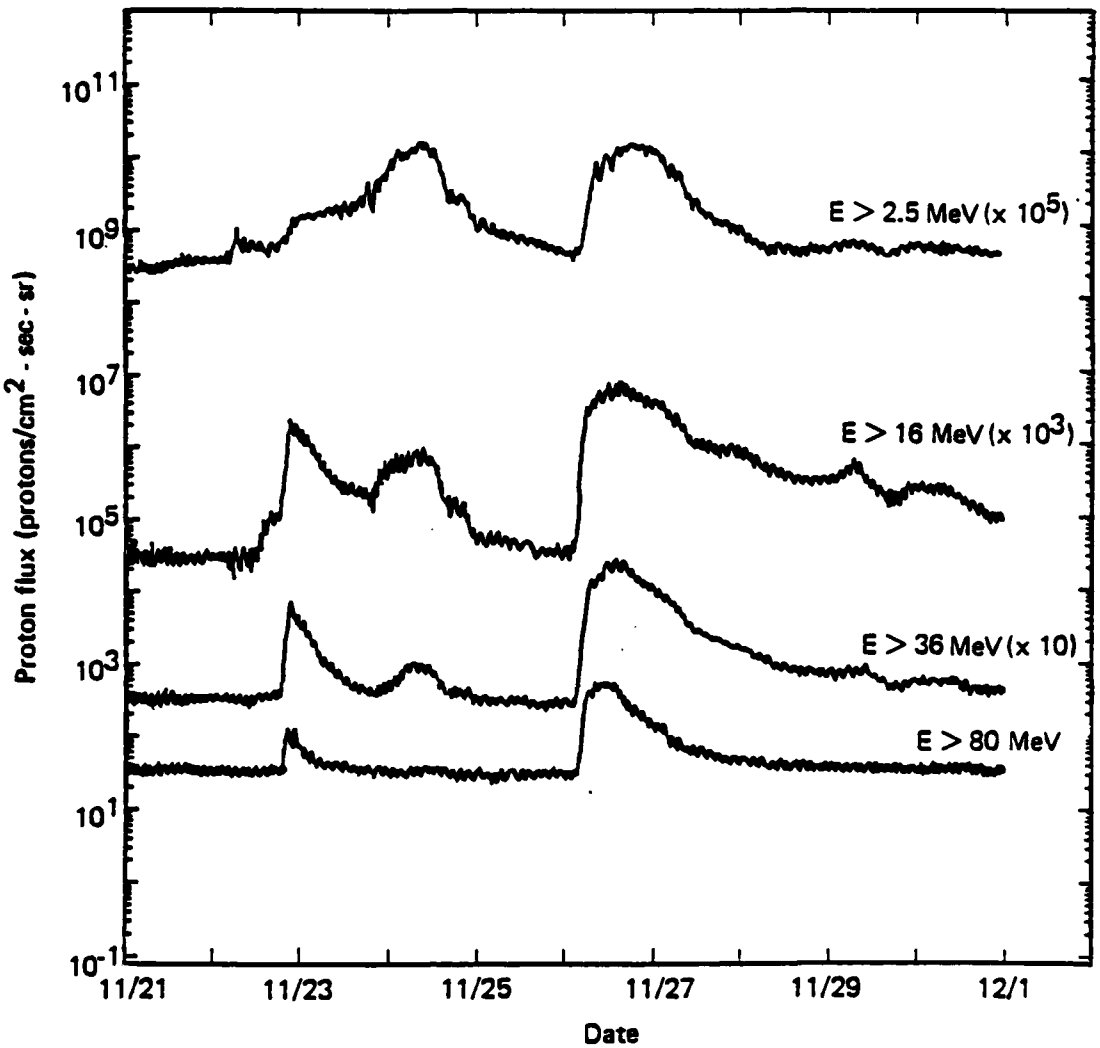

Fig. 3--Integral proton fluxes averaged over geomagnetic latitudes greater than 70 deg (NOA66 satellite measurement)

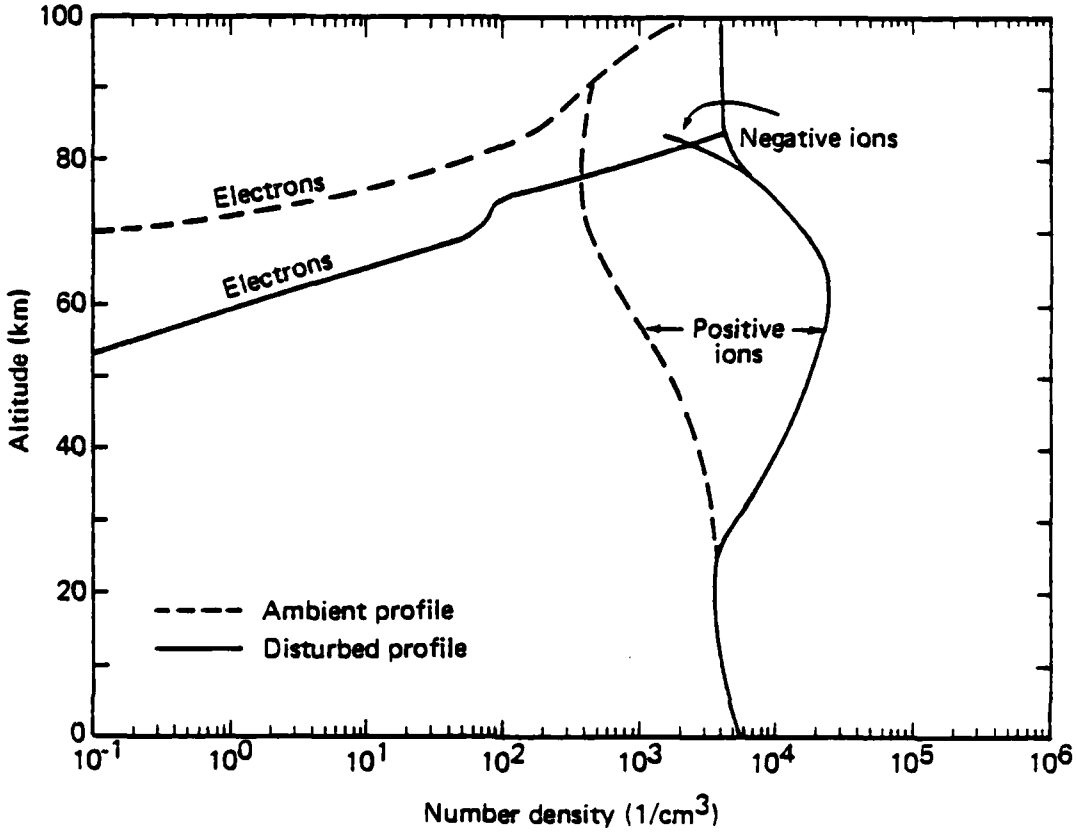

Fig. 4--Electron and ion densities at 0800 UT:
23 November 1982

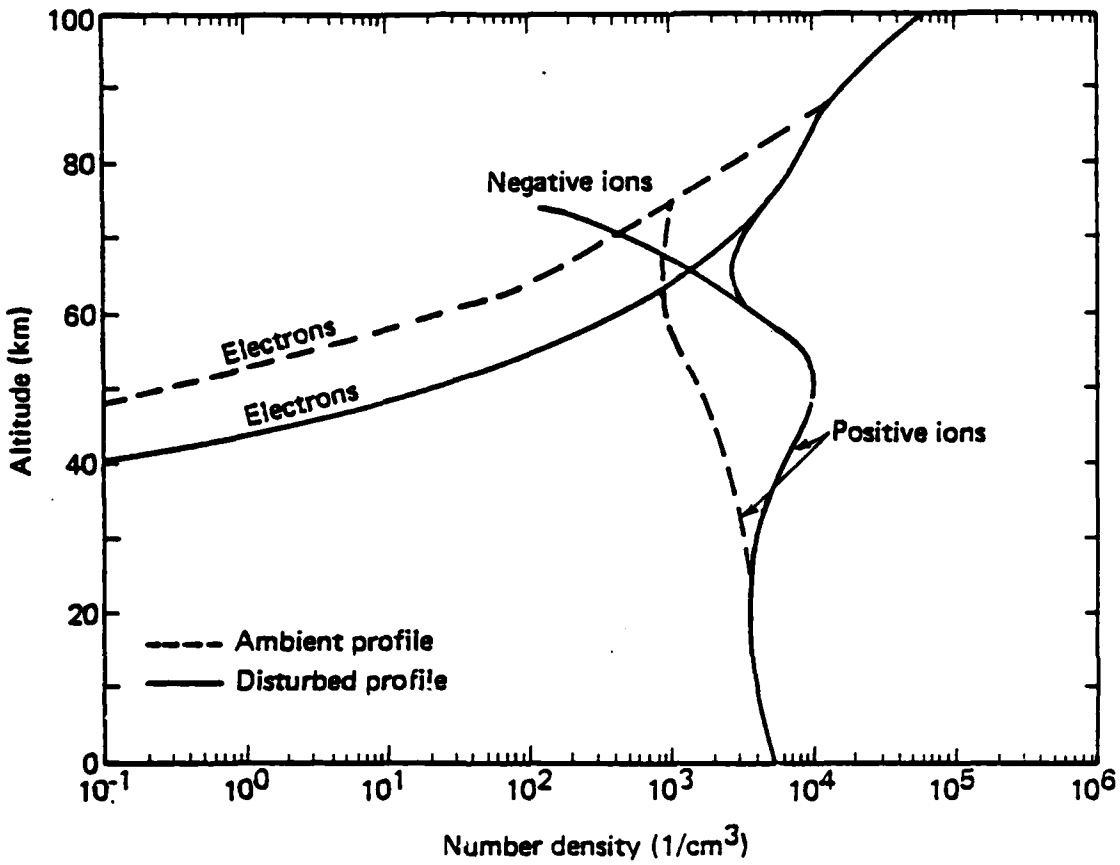

Fig. 5--Electron and ion densities at 1600 UT:
23 November 1982

IV. PROPAGATION MODEL OF NOVEMBER 1982 SPE

This section demonstrates that the ELF anomalies shown in Fig. 2 are too large to be explained by increased attenuation along the great-circle propagation path. It then uses measured proton fluxes to develop a model of the nonstratified polar cap that is employed in Secs. V and VI.

Propagation in Stratified Waveguide

The equations governing ELF propagation for laterally uniform conditions are available from many sources, e.g. Galejs [1972]. To define the notation and illustrate the key dependences, the equation for the spatial dependence of the fields is recapitulated. The expression for the horizontal magnetic intensity H is

$$H_\phi = A\,(\Lambda_T\Lambda_R)^{1/2}\left(\frac{c}{v}\,d\right)^{-1/2} \exp\left(-\frac{2\pi i}{\lambda}\,\frac{c}{v}\,d\right) e^{-\beta d/8.7} \cos\phi \quad \text{A/m}, \qquad (1)$$

where A depends on the antenna moment, frequency, and ground conductivity, but not on the ionosphere; λ is the wave length in megameters; and ϕ is the angle between the propagation path and the end-fire direction. The excitation factors are Λ_T and Λ_R at the transmitter and receiver locations, c/v is the relative phase velocity, β is the attenuation rate in decibels per megameter of propagation, and d is the distance from the source in megameters.

The amplitude of a long-range ELF signal is most sensitive to changes--first in the attenuation rate β, and second, in the excitation factor Λ. The phase depends mainly on c/v.

In the idealized limit of a perfectly reflecting, sharply bounded ionosphere at a height H_0 above the ground, the excitation factor Λ is equal to $1/H_0$. Even for diffuse ionospheric boundaries, as treated in this report, the magnitude of Λ is of the same order as the reciprocal of the nominal ionosphere reflection heights. Thus, an ionospheric disturbance that lowers the effective height will increase Λ.

The ELF data shown in Fig. 2 compare the amplitude and phase of the signal during the 23 November SPE with the amplitude and phase of the signal under average undisturbed conditions. Therefore, to avoid complexity, the difference between the ambient and disturbed signals was computed instead of the signals themselves.

Equation (1) can be used to derive the simple expression given below for the SPE-induced amplitude changes ΔH_ϕ, and phase changes $\Delta\theta$. This can be done if we ignore minor phase variations in Λ and c/v which, strictly speaking, have complex values with small imaginary parts, and if we ignore the minor dependence of amplitude on c/v.

$$\Delta H_\phi = (\beta - \beta^{SPE})D + 10 \log (\Lambda_T^{SPE}\Lambda_R^{SPE}/\Lambda_T\Lambda_R) \quad \text{dB}, \tag{2}$$

$$\Delta\theta = 91.7\left[c/v - (c/v)^{SPE}\right] D \quad \text{deg.} \tag{3}$$

Quantities corresponding to SPE-disturbed conditions are indicated by the superscript SPE. The length of the propagation path that lies beneath the disturbed cap is given by D. Equations (2) and (3) apply when the earth-ionosphere waveguide behaves as though it were nearly stratified.

Calculated Propagation Parameters

The literature supplies full-wave methods for calculating β, c/v, and Λ for virtually any ionospheric height profile, as well as numerical results for many models of ambient and disturbed ionospheres [Budden, 1961a; Field, 1970; Wait, 1970; Galejs, 1972; Pappert and Moler, 1974; Greifinger and Greifinger, 1978]. The profiles of Figs. 4 and 5 were used as input to the Pacific-Sierra Research Corporation (PSR) full-wave computer code [Field, 1970]. This code calculates the propagation parameters under the center of the polar cap and under ambient conditions. Table 1 lists the results of those calculations.

Equations (2) and (3) assume a nearly stratified waveguide and do not apply to the geometry shown in Fig. 1. However, they can be used to obtain an upper bound on the anomalous attenuation that the signal

Table 1

Calculated propagation parameters at 76 Hz

Date	Time (UT)	β(dB/Mm)	c/v	$\Lambda(m^{-1})$
Ambient	Night	0.87	1.14	7.5×10^{-6}
23 November 1982	0800 (night)	1.62	1.24	9.2×10^{-6}
Ambient	Daylight	0.94	1.19	9.2×10^{-6}
23 November 1982	1600 (daylight)	1.28	1.24	1.0×10^{-5}

could have suffered propagating on a great-circle path from the WTF to the Gulf of Alaska. To obtain that bound, only the first term on the right side of Eq. (3) is retained. This is equivalent to the assumption that the entire path is beneath the disturbed polar cap while the terminals are under ambient conditions. We overstate the exposed path length and ignore possible enhancement. This enhancement is caused by the ionosphere being lowered over either terminal, thus increasing the excitation factors.

Insertion of the attenuation rates from Table 1 and the value D = 3.5 Mm into Eq. (2) gives ΔH_ϕ = -2.6 dB and ΔH_ϕ = -1.2 dB under night and daylight conditions, respectively. These calculated signal losses, which are upper bounds, are smaller than the measured values of 3 to 4 dB and 2 dB (see Fig. 2). In fact, the discrepancy between the measured losses and the ones calculated from stratified-waveguide theory is greater than indicated by the figures because (1) the entire great-circle path was not exposed to the central polar cap, and (2) the terminals were so close to the polar cap boundary that some increase in excitation factor (say, one-half of the values shown in Table 1) would be expected. If those adjustments are made, Eq. (2) predicts virtually no signal loss in the daylight and about 1 dB loss at night. Moreover, Eq. (3) predicts a -32 deg phase shift at night

and a -16 dB phase shift in daylight, but virtually no phase shifts were observed.

These results show that the measurements cannot be explained by a theory that omits lateral refraction, reflection, and diffraction at the boundary of the disturbed polar cap.

Polar Cap Boundary Model

In order to model the polar cap boundary, measurements of the proton flux versus geomagnetic latitude are needed. Because the data for the 23 November SPE reveal only the time dependence of the flux averaged over the cap, the latitudinal dependence must be inferred from data measured during other SPEs. For example, Fig. 6 shows the flux versus latitude for the 8 December 1982 event. The fluxes are approximately constant above 60 deg and fall off at a fairly constant rate between about 60 and 50 deg. Therefore, we assume the disturbed polar cap to be uniform between the north geomagnetic pole and 60 deg latitude, which is about 3.0 Mm from the pole. The diffuse boundary, or transition zone, extends to 50 or 55 deg and is 0.5 to 1 Mm wide. Both WTF and the Gulf of Alaska are at about 55 deg north geomagnetic latitude and are in the boundary region.

We assume a flat earth, an isotropic ionosphere, symmetry about the north geomagnetic pole, and model the propagation constant as:

$$S(x, y) = S_{SPE} + (S_{AMB} - S_{SPE})/\{1 + \exp[-(r - r_0)/\delta r]\}, \qquad (4)$$

where S is related to the phase velocity and attenuation rate by the formulas $c/v = \mathrm{re}S$, and $\beta = -8.6k\ \mathrm{im}S$. In addition, S_{AMB} and S_{SPE} denote the values of S under ambient and disturbed conditions, respectively. The distance from the pole is r, r_0 is the radius of the center of the polar cap boundary, and δr is a scale distance that we use below to define the width of the boundary. Figure 7 diagrams this model and defines some parameters.

If the boundary width Δr is defined as the distance over which S undergoes 95 percent of its transition from disturbed to ambient, and

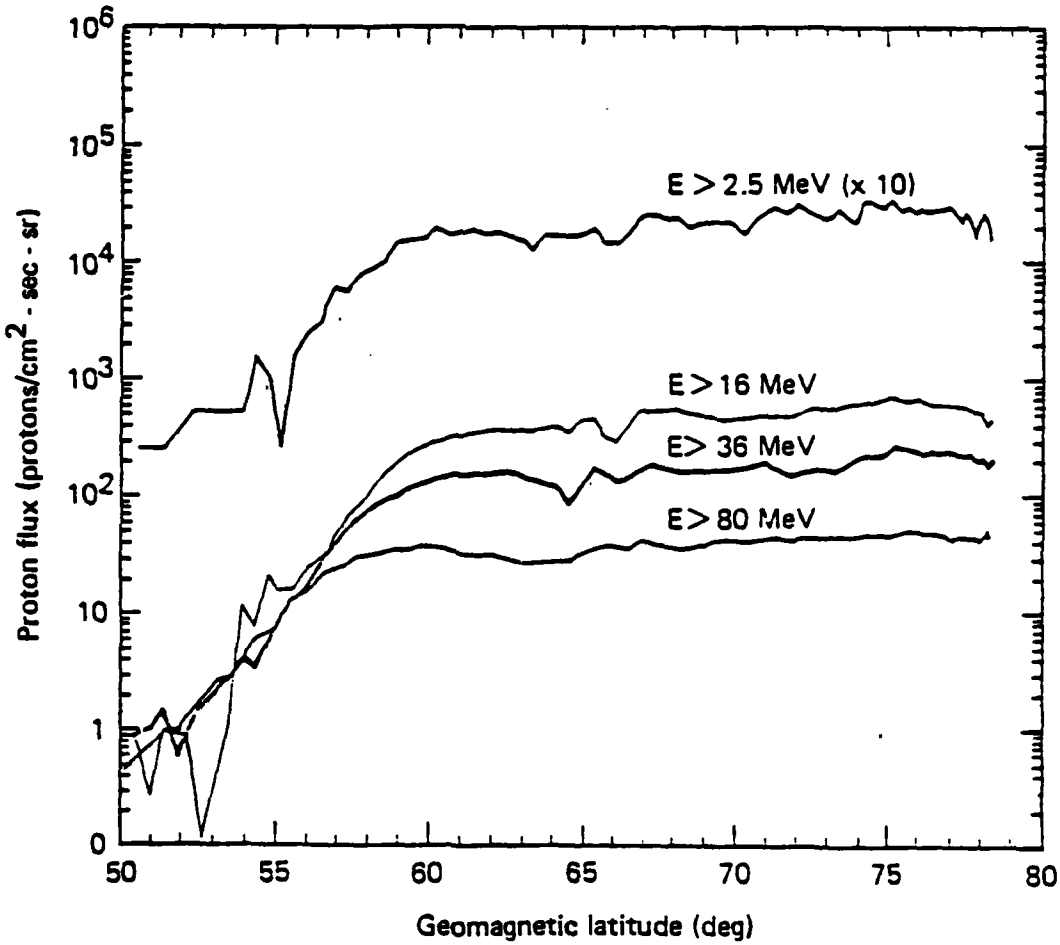

Fig. 6--Integral proton fluxes versus geomagnetic latitude: 8 December 1982

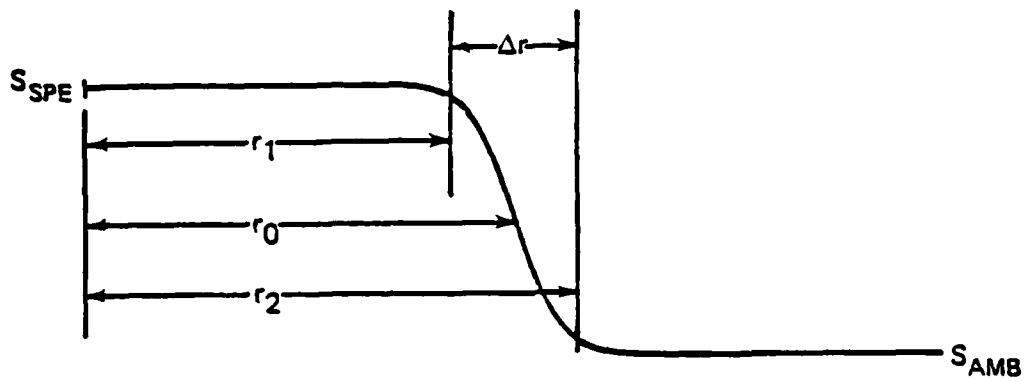

Fig. 7--Model of polar cap propagation constant

r_1 and r_2 are the inner and outer radii of the boundary region, respectively, it follows that (see Appendix B)

$$r_2 = r_1 + \Delta r \quad , \tag{5}$$

$$r_0 = (r_1 + r_2)/2 \quad , \tag{6}$$

$$\Delta r = 7.3\ \delta r \quad . \tag{7}$$

The transmitter-to-receiver path length is 3.5 Mm on a great-circle path. We will assume that the Gulf of Alaska receiver is approximately the same distance from the north geomagnetic pole as the WTF transmitter. Since the exact location of the receiver is not certain, we will regard the gulf as a 1 Mm square area, the center of which is 3.5 Mm, from both the WTF and the north geomagnetic pole. We will assign r_1 the value of 3.0 Mm, which allows the model of the propagation medium in Fig. 8.

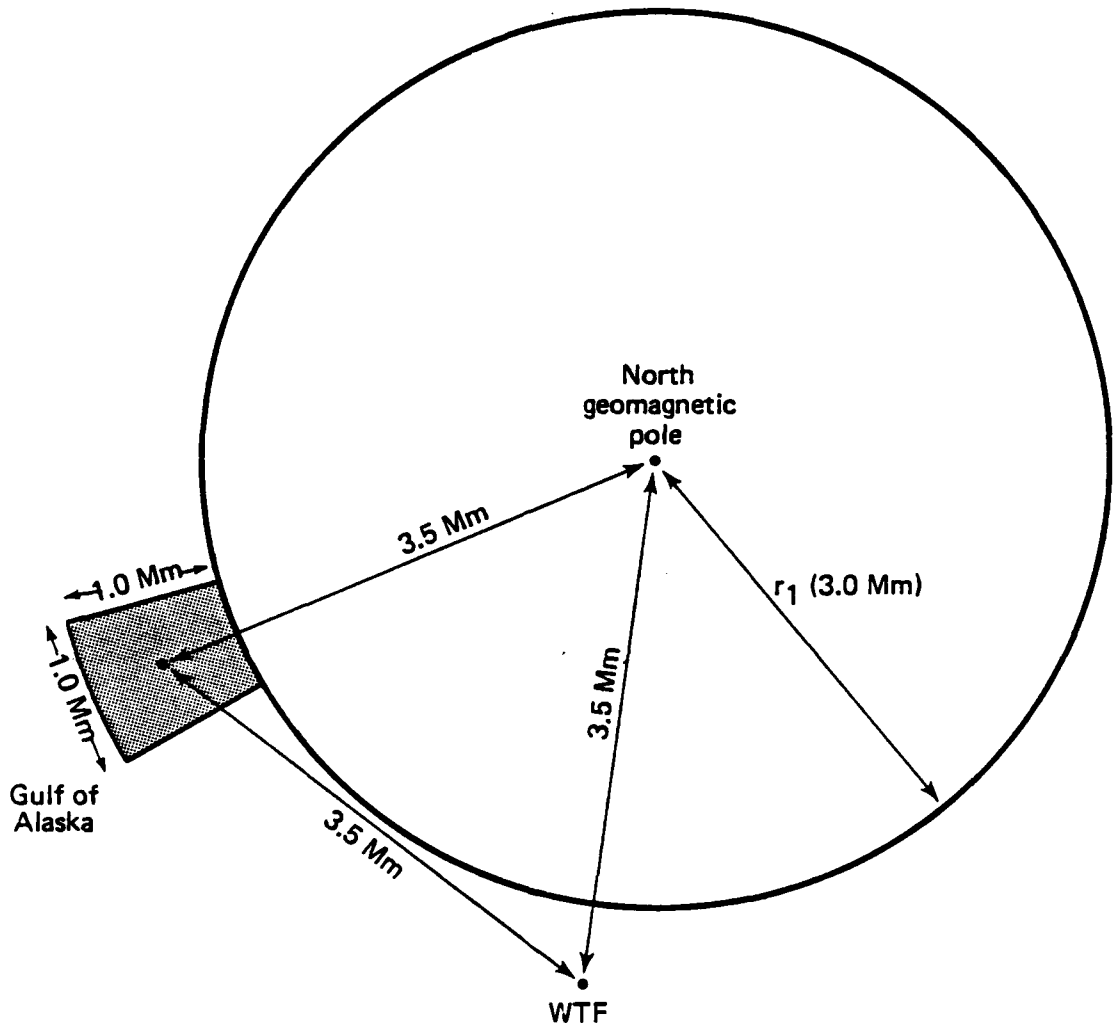

Fig. 8--Schematic of propagation model

V. TWO-DIMENSIONAL RAY TRACE: LATERAL REFRACTION OF TEM MODE

The WTF and Gulf of Alaska are at about 55 deg geomagnetic north latitude and probably lie in the boundary region, where strong transverse gradients in S will refract the field. More simply, the propagation constant S behaves as a refractive index and tends to bend the fields toward the inner cap, where the phase velocity is slowest. Under the proper conditions, this effect could create a shadow zone to which rays emanating from the WTF cannot gain access.

To test this hypothesis a simple ray trace is used. It is summarized in this section and derived in Appendix B. The results are only semiquantitative, because the validity criterion for ray tracing is marginally satisfied for most of the assumed boundaries and is actually violated for the abrupt ones. Therefore, ray tracing will overstate the refraction. In Sec. VI, the fields are recalculated using a full-wave integral equation.

We assume a two-dimensional propagation medium, whose propagation constant S is given by Eq. (4). Because the propagation constant is analogous to a refractive index, the problem is mathematically identical to tracing rays that are obliquely incident on an isotropic ionosphere that varies in two dimensions, but is uniform in the direction perpendicular to the plane of propagation. To isolate refractive effects, we ignore the imaginary part of S and, hence, absorption. Signal anomalies calculated in this fashion are caused solely by lateral focusing or defocusing of the TEM mode.

The following geometric parameters are assumed:

$$r_1 = 3 \text{ Mm} \quad , \tag{8}$$

$$\Delta r = 1 \text{ Mm} \quad . \tag{9}$$

Rays are traced for a total of six levels of disturbance, including: (1) weak, equivalent to the 23 November 1982 SPE, characterized by

reS_{SPE} = 1.25, (2) moderate, a bit stronger than the 8 December 1982 SPE, characterized by reS_{SPE} = 1.35, and (3) very strong, characterized by reS_{SPE} = 1.50. In each case ambient conditions are characterized by reS_{AMB} = 1.15, which corresponds to nighttime propagation.

A top view of the ray trajectories is diagrammed in Fig. 9. In all cases the rays bend toward the polar cap and become less dense in the southern Gulf of Alaska, shown as the shaded area. The signal is weakest where the rays are least dense and strongest where they are densest. As is to be expected, the refraction increases as the SPE becomes stronger. For all but the weakest of the modeled events, a caustic is formed near the inner edge of the boundary region.

Figure 10 reveals the dependence of the ray trajectories on the thickness of the boundary. Those results were calculated for the weak SPE (S = 1.25) and boundary thicknesses ranging from 0.5 to 1.0 Mm. As before, the radius of the inner polar cap is assumed to be 3.0 Mm. The results given in Figs. 9 and 10 show that the signal depends strongly on the boundary thickness as well as on the strength of the disturbance.

The effects of an SPE on signal pattern (shown in Figs. 9 and 10) would be azimuthally symmetric if the ionosphere were stratified. Figures 9 and 10 indicate the difference between the actual field in a region, and what would have been received if the WTF radiation pattern were not distorted by lateral refraction. Although the ray trace is a convenient means of estimating the locations and relative strengths of signal concentrations and rarefactions, Figs. 9 and 10 cannot be used to compare ambient fields with those measured during an SPE. That calculation would require each ray to be weighted by a number that accounts for the waveguide excitation factor.

Figures 9 and 10 show that lateral refraction can be substantial. It is estimated that,* for a 1-Mm thick boundary, refraction changes the signal in the southern Gulf of Alaska -8 dB relative to a symmetric signal for the strong SPE; -3.5 dB for the moderate SPE; and

---

* The received field is inversely proportional to the square root of the distance between rays.

-1.4 dB for the weak SPE. These effects increase as the boundary becomes more abrupt. For the weak SPE, which corresponds to the 23 November event, the ray trace predicts that defocusing in the southern Gulf of Alaska is as much as -6 dB for the narrowest boundary (0.5 Mm) and -2 dB for a boundary width of 0.7 Mm. Note that these refractive effects are over and above losses attributable to attenuation.

The field depends strongly on receiver location. For all cases shown, a region of intensification (focusing) occurs just a few hundred kilometers north of the region of minimum field. Since the exact location of the submarine-borne receiver is unknown, a detailed comparison cannot be made between experiment and theory. The concept of energy refracting away from the Gulf of Alaska and into the polar cap appears consistent with the measured SPE-induced signal loss that was too severe to have been caused by attenuation alone.

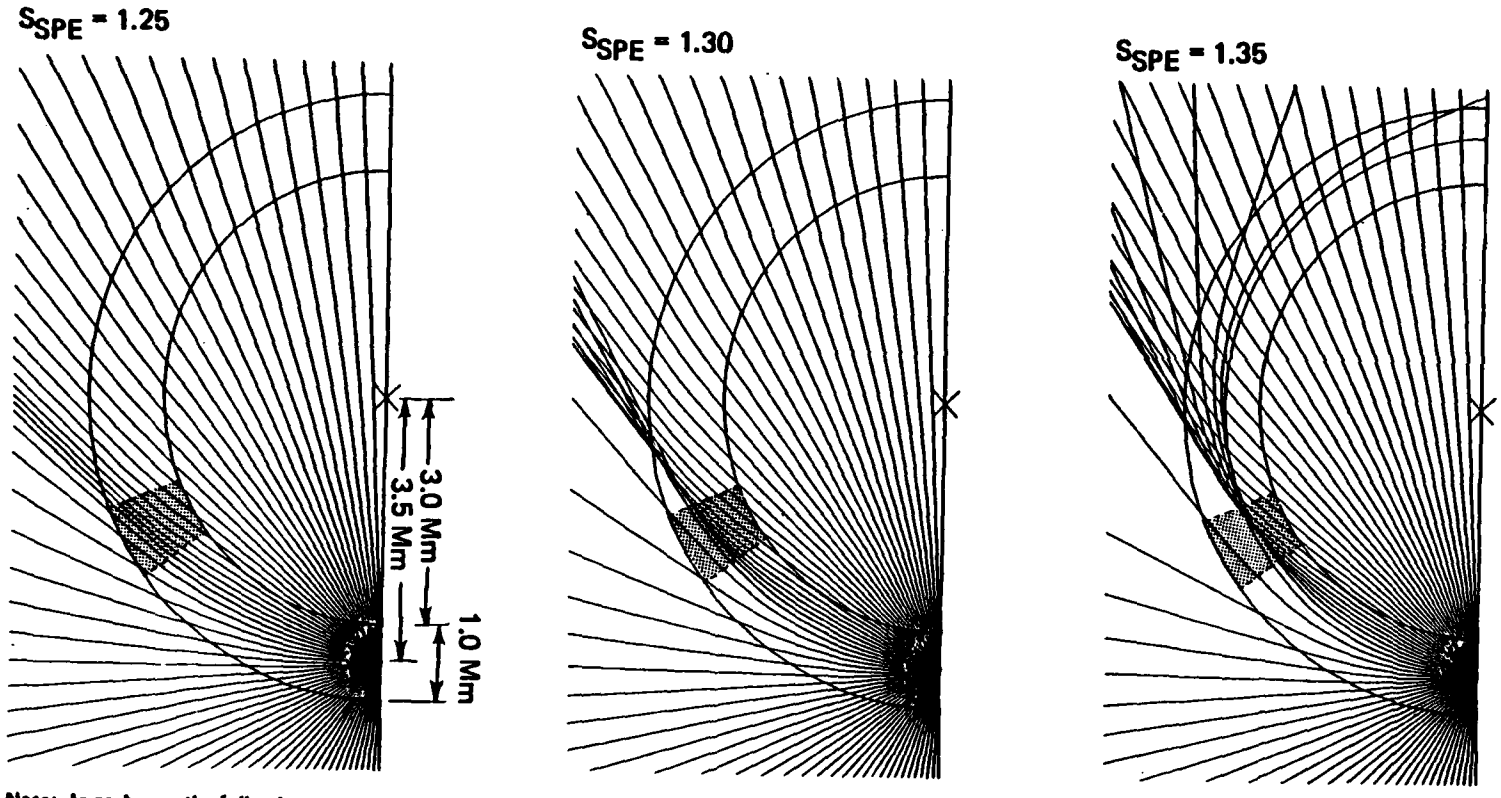

Note: In each case the following values apply:
- S_{AMB} = 1.15, Transmitter = 3.5 Mm from center of disturbance, and Edge of constant region = 3.0 Mm from center of disturbance.

Fig. 9--Ray tracing for SPEs of various strengths

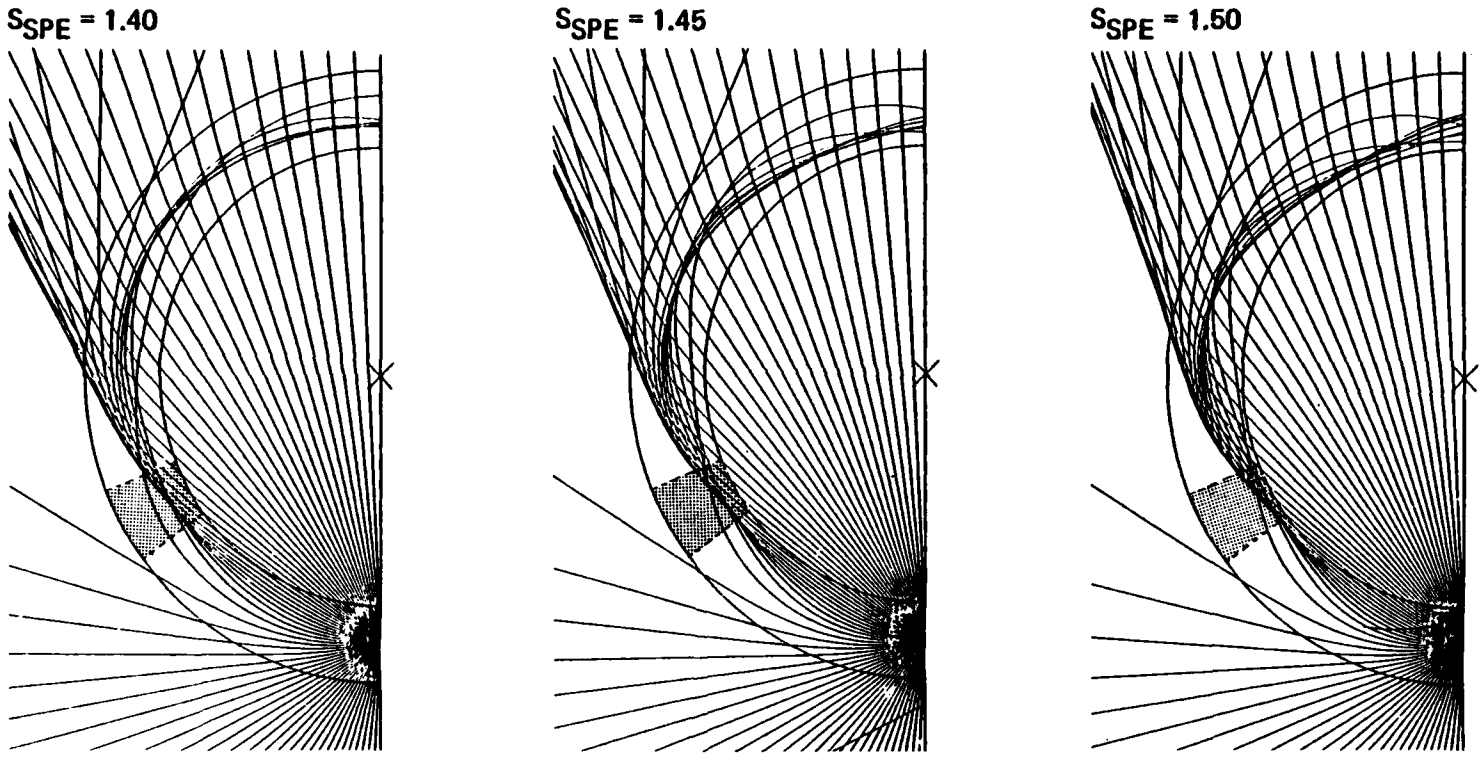

Fig. 9--Continued

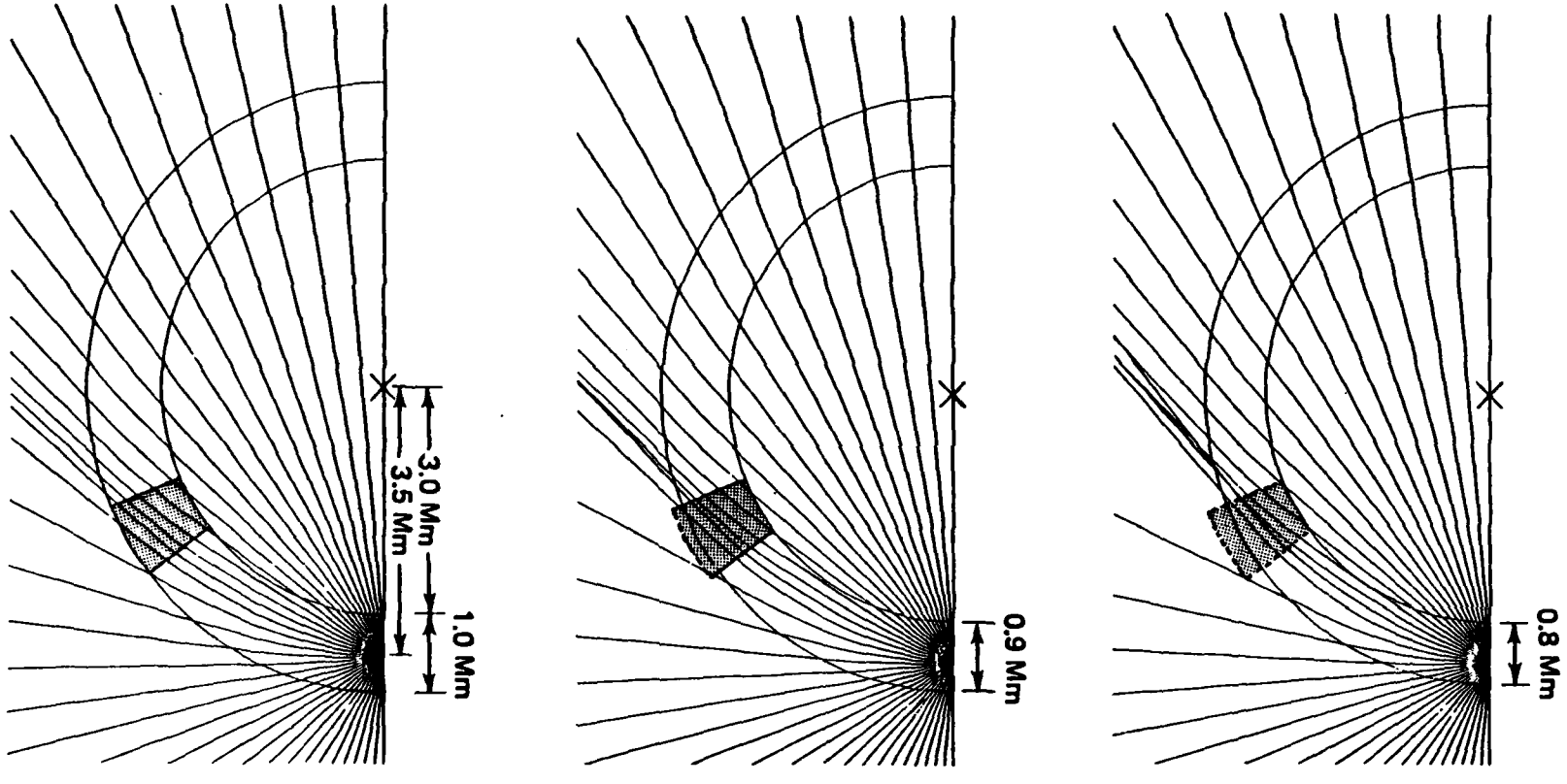

Note: In each case the following values apply:
S_{SPE} = 1.25, S_{AMB} = 1.15, Transmitter = 3.5 Mm from center of disturbance, and Edge of constant region = 3.0 Mm from center of disturbance.

Fig. 10--Ray tracing for weak SPE and various transition zone widths

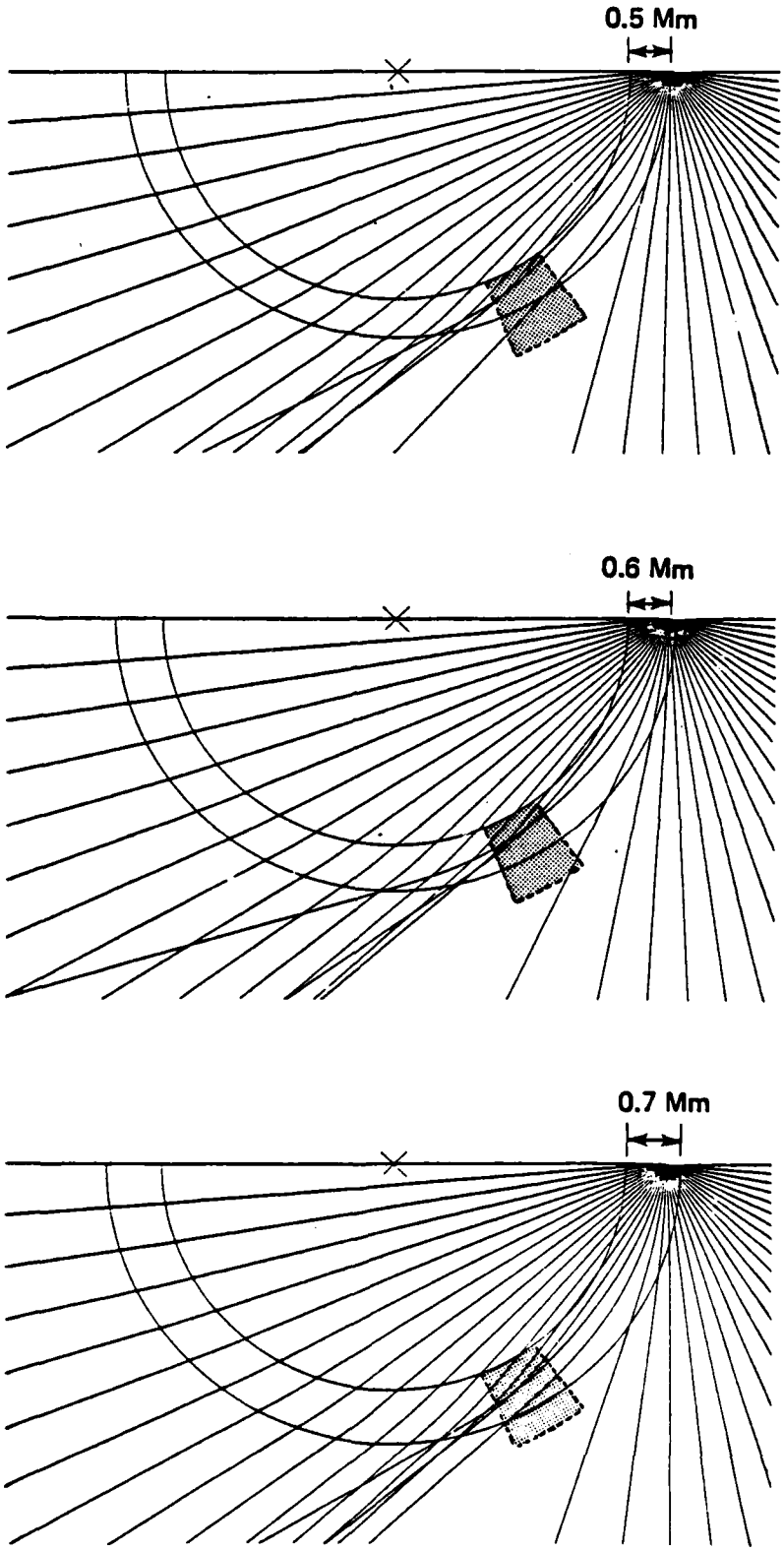

Fig. 10--Continued

VI. FULL-WAVE CALCULATIONS USING INTEGRAL WAVE EQUATION

This section presents results calculated from an integral equation developed by Field and Joiner [1979] to analyze ELF propagation under conditions where the earth-ionosphere waveguide is not stratified. That full-wave equation accounts for a number of phenomena that the ray trace omits, including attenuation, diffraction, and lateral reflection. A major disadvantage of the equation is the large computer expense needed to achieve a solution. Therefore, only a few sample cases are shown below. Concentration is on effects caused by diffraction and reflection.

Integral Wave Equation

Field and Joiner [1979] write the field at the ground as

$$E = A\,\Lambda(x, y)\,\Psi(x, y)\,F(z) \quad , \tag{10}$$

where A is a constant involving dipole moment, wave frequency, and ground conductivity; Λ is the excitation factor and a function of position; F is the vertical dependence; and Ψ is the lateral dependence of the signal. The lateral dependence can be found by solving

$$[\nabla_T^2 + k^2 S^2(x, y)]\,\Psi = 0 \quad , \tag{11}$$

where

$$\nabla_T^2 = \frac{\partial^2}{\partial x^2} + \frac{\partial^2}{\partial y^2} \quad .$$

Here S is the propagation constant and is found by imposing boundary conditions on F(z) at the ground and in the ionosphere.

The WTF consists of two nearly perpendicular horizontal dipoles. Katan and Bannister [forthcoming] report that the phase difference between the two antenna elements was 290 deg during the 23 November tests. That phase angle gives a radiation pattern that, for the pur-

poses of the present report, can be assumed symmetric. If we further assume the transmitter to be at the origin of a cylindrical coordinate system, then for a stratified waveguide where $S^2(x, y) = S_0$, the solution of Eq. (11) is

$$\Psi = H_0^{(2)}(k\ S_0\ r) \quad , \tag{12}$$

where r is the distance from the origin, and H is the Hankel function.

Strictly speaking, the separation of variables that leads to the solution given by Eq. (12) is invalid when the ionosphere is not stratified. However, under most conditions the eigenvalue S is governed primarily by the local ionosphere. That assumption allows the solution to Eq. (10) to be written in the form

$$\Psi = W(x, y)\ H_0^{(2)}(k\ S_{AMB}\ r) \quad , \tag{13}$$

where W(x, y) is a propagation factor that is unity under undisturbed conditions and gives the relative effect of a nonstratified disturbance on the signal. A lengthy derivation [Field and Joiner, 1979] reveals that W(x, y) satisfies the following integral wave equation:

$$W(x, y) = 1 - \frac{ik^2}{4}\iint dx'\ dy'\ \left[S^2(x, y) - S_{AMB}^2\right] \times \frac{H_0^{(2)}\left(k\ S_{AMB}\ r_2\right) H_0^{(2)}\left(k\ S_{AMB}\ r_1\right)}{H_0^{(2)}(k\ S_0\ r)}\ W(x', y') \quad , \tag{14}$$

where

$$r^2 = x^2 + y^2 \quad ,$$

$$r_1^2 = (x')^2 + (y')^2 \quad ,$$

$$r_2^2 = (x - x')^2 + (y - y')^2 \quad .$$

Numerical Results

As was done for the ray-trace calculations presented in Sec. IV, the propagation constant S is given by Eq. (4), and only reS is retained which is tantamount to neglecting attenuation. Any SPE-induced signal changes calculated in this manner are caused by refraction, reflection, or diffraction at the boundary. The changes are over and above losses caused by attenuation. The results given below are more accurate than those given in the previous section, because the ray trace is not fully valid for all boundary thicknesses treated, and it breaks down near caustics.

Contour plots of the change in W caused by a weak SPE having boundary thicknesses of 0.5 and 1 Mm, respectively, are illustrated in Figs. 11 and 12. Those parameters represent the 23 November event. The figures show, in decibels, the signal during the event relative to the signal during ambient night. Figure 13 is analogous to Figs. 11 and 12, but applies to a strong SPE with a 1-Mm boundary thickness. Note that for a stratified ionosphere, the contours would be azimuthally symmetric about the transmitter.

The results are qualitatively similar to the ray traces. In all cases there is a signal increase in the northern gulf where the ray trace produced a caustic, and a signal decrease in the southern gulf where the ray trace showed a decrease in ray density. Presumably, that decrease corresponds to the anomalous signal loss measured during certain SPEs.

The signal distortions shown in Figs. 11 through 13 are not as strong as those given by the ray trace, which, for reasons given above, overstates the refraction.

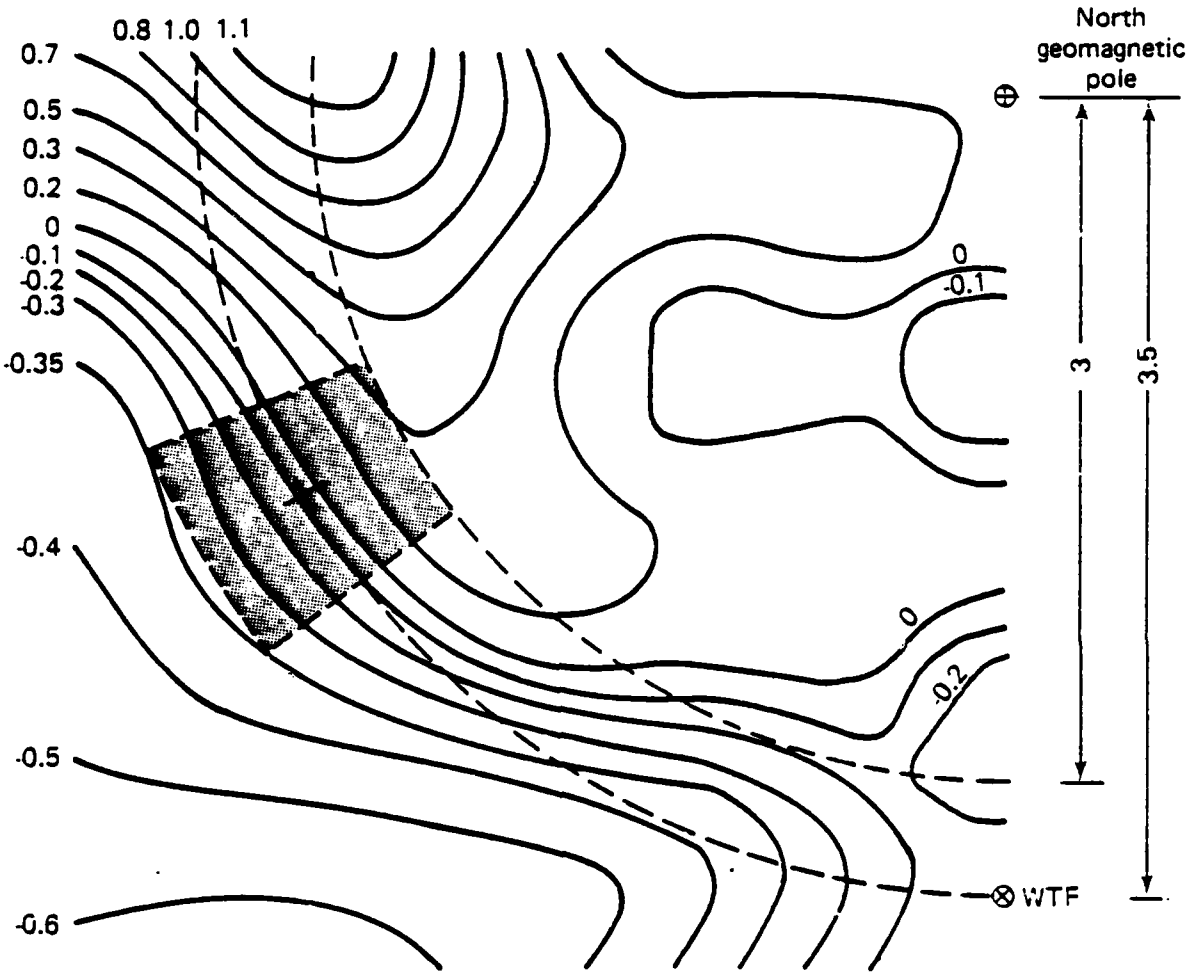

Fig. 11--Contour plot of |W| in dB//1 for weak SPE, S_{SPE} = 1.25 (transition zone width = 0.5 Mm)

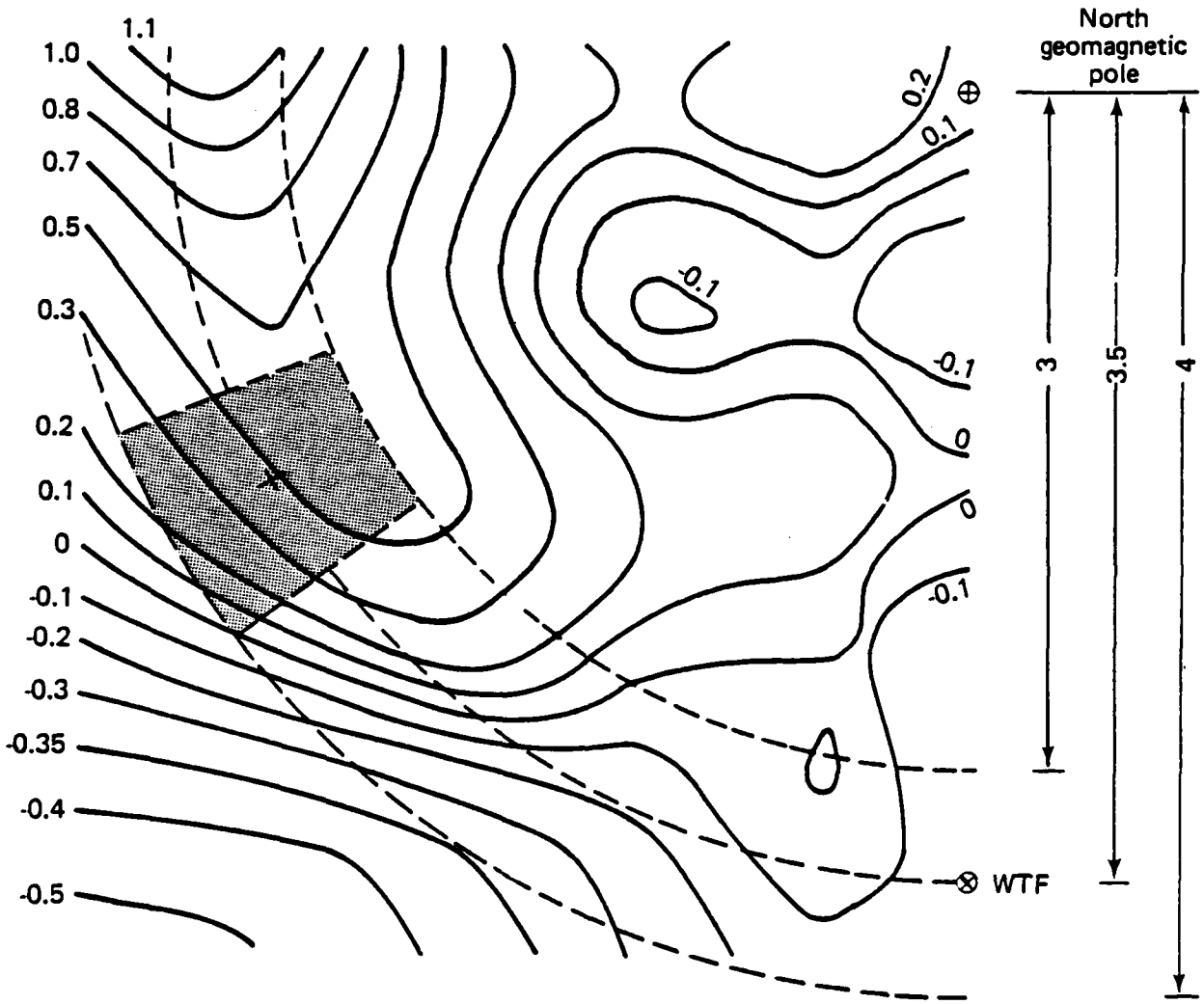

Fig. 12--Contour plot of |W| in dB//1 for weak SPE, S_{SPE} = 1.25 (transition zone width = 1 Mm)

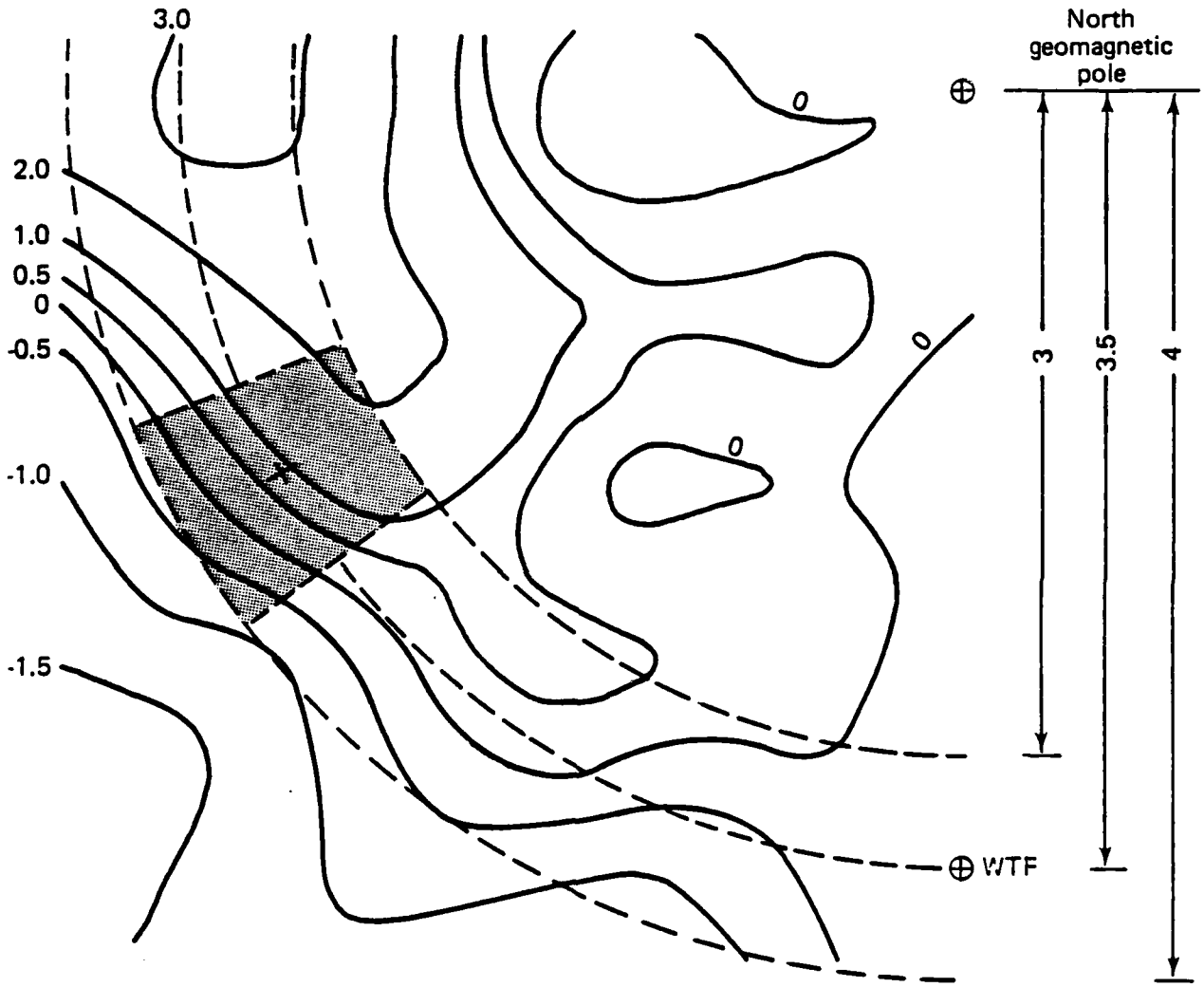

Fig. 13--Contour plot of |W| in dB//1 for strong SPE, S_{SPE} = 1.45 (transition zone width = 1 Mm)

VII. CONCLUSIONS

In order to interpret anomalous signal losses measured during several SPEs, two methods were developed for handling ELF propagation near lateral nonhomogeneities in the earth-ionosphere waveguide: (1) a full-wave integral equation that is accurate, but expensive to solve, and (2) a two-dimensional ray trace that provides physical insight, although it is only semiquantitative.

Both methods were applied to several model SPEs, including one based on the 23 November 1982 event, which is of special interest because simultaneous measurements of ELF signal anomalies and incident proton fluxes are available. All calculations indicated a region of weak field in the southern Gulf of Alaska, where a submarine-borne receiver measured an unusually severe signal loss. That behavior is caused by lateral refraction, which distorts the WTF radiation pattern by bending energy away from the gulf and into the disturbed polar cap, where the phase velocity of the TEM mode is lowest. Accordingly, the theory also predicts a region of strong field just inside the polar cap boundary, but no data are available to test that result.

Localized regions of weak or strong fields are by no means restricted to situations where the great-circle propagation path grazes the edge of the polar cap, as was the case for the WTF to Gulf of Alaska link considered here. They will occur on any link where the great-circle path is nearly tangent to a boundary between large zones with different ionospheric or ground properties and, hence, different waveguide phase velocities. Examples of such boundaries include the terminator and the Greenland shoreline.

Appendix A

CALCULATION OF IONIZATION PROFILES FROM PROTON FLUXES

In this appendix we discuss the calculation (using proton flux data) of the ionospheric charged particle densities. First, the proton data are used to determine rates of ion-pair production at altitudes that affect ELF propagation. Second, those rates are input to air-chemistry equations to obtain height profiles of electron and ion densities.

Calculation of ion-pair production rates requires knowledge of the proton flux in a large number of narrow energy bins between about 1 and 300 MeV. To find the number of protons at energy E or greater the National Oceanic and Atmospheric Administration (NOAA) fits the four coarse energy bands of the spacecraft data to the following empirical formula for the integral proton flux:

$$J = J_0 \, e^{-R/R_0} \quad \text{protons/cm}^2\text{-sec-sr} \quad , \tag{A.1}$$

where

$$R = E^2 + 2EE_0 \quad \text{MeV} \quad . \tag{A.2}$$

In the above equations, E_0 is the proton rest energy (936 MeV), and J_0 and R_0 define the strength and energy rigidity, respectively, of the integral flux.

The values of J_0 and R_0 supplied by NOAA for 23 November 1982 are shown in Fig. A.1. The strength J_0 changes by a factor of about 2 during the daylight and night periods. The rigidity R_0, however, changes little. In fact, even the models generated using R_0 for different times during daylight and night show little difference.

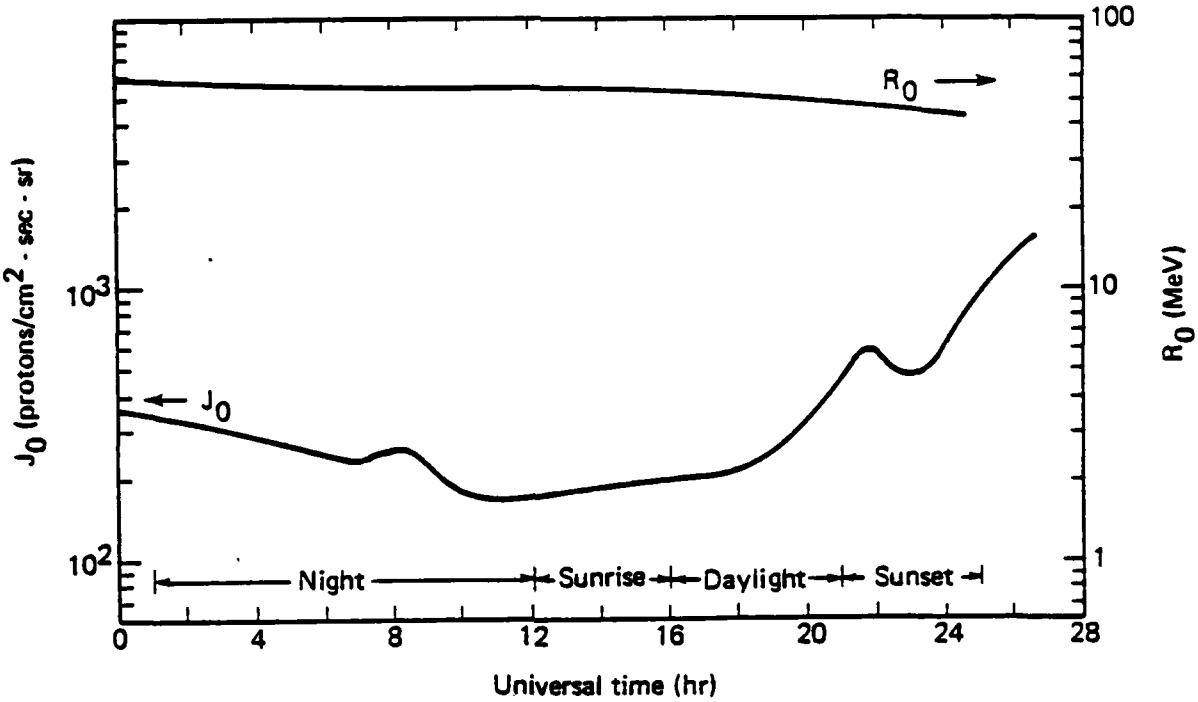

Fig. A.1--Strength and rigidity parameters:
23 November 1982

In Fig. A.2 [Reid, 1978], profiles of ion-pair production rates per proton are presented for isotropic fluxes of monoenergetic protons of given energies. To find the total production rate, the number of protons of a particular energy must first be found. It is assumed that all the protons in a range of energy have the same nominal energy. If E_{min} and E_{max} are the minimum and maximum energies of the range, respectively, then the total number of protons at the nomimal energy is given by

$$J_{total} = J(E_{min}) - J(E_{max}) \quad .$$

Table A.1 lists the energy ranges and the nominal energies used in this report. Logarithmic spacing is employed.

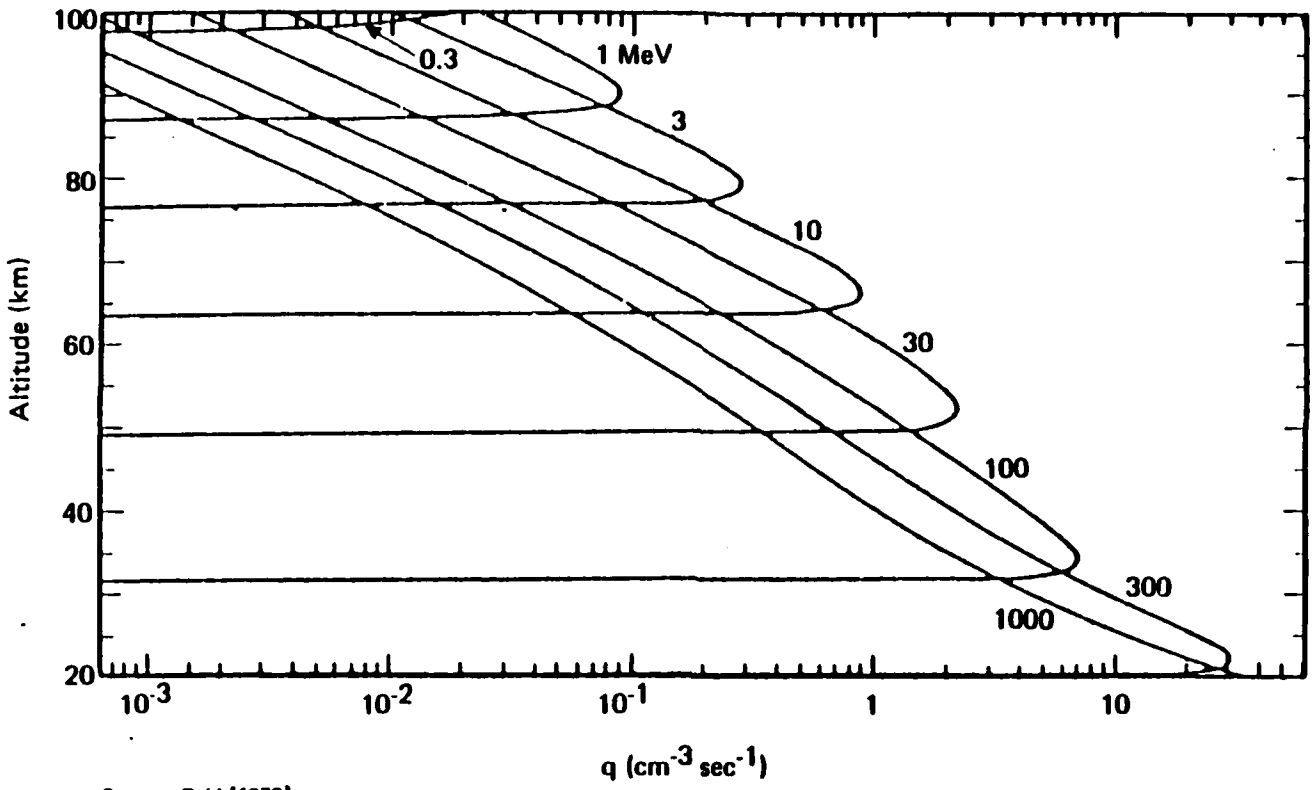

Source: Reid (1978).

Fig. A.2--Ionization per proton of given energy

Table A.1

Energy bands used to find ion-pair production rates (In MeV)

Energy Range[a]	Nominal Energy
0.6 - 2.0	1.0
2.0 - 6.0	3.0
6.0 - 20.0	10.0
20.0 - 60.0	30.0
60.0 - 200.0	100.0
200.0 - 600.0	300.0
600.0 - 2000.0	1000.0

[a]Includes protons that deposit their energy and, hence, produce ionization, at altitudes between 15 and 110 km.

Table A.1 and Eq. (A.1), as well as Fig. A.1 allow us to find the production rates q. These rates are then inserted into the three-species, lumped parameters deionization model of Knapp and Schwartz [1975]. They give the following for the electron density N_e and the positive ion density N_+ at altitude h:

$$N_e(h) = \frac{(q + D)}{[A + D + \alpha_d N_+(h)]} , \tag{A.3}$$

$$N_+(h) = \frac{q}{\alpha} , \tag{A.4}$$

where

$$\alpha = \frac{\left\{A\alpha_i + D\alpha_d + \alpha_i\alpha_d\left[\frac{q(A + D)}{A\alpha + D\alpha}\right]^{1/2}\right\}}{\left\{A + D + \alpha_i\left[\frac{q(A + D)}{A\alpha + D\alpha}\right]^{1/2}\right\}} , \qquad (A.5)$$

In the above equations A, D, α_i, and α_d are functions of altitude and pair production, and are taken from figures in Knapp and Schwartz [1975]. Their simple air-chemistry model, developed under Defense Nuclear Agency auspices, has for years been the standard method of calculating ionospheric ionization produced by radiation from high-altitude nuclear bursts. However, more detailed models that account for large numbers of ionospheric species do exist, although the values for the deionization coefficients, though widely used, are not precise.

The pair production rates are smoothed before insertion into Eqs. (A.3) through (A.5). The results are shown in Figs. 4 and 5 on pp. 10 and 11. The particle densities, as well as the collision frequencies, mean ionic mass, and geomagnetic field strength must be specified in order to define the electromagnetic properties of the ionosphere. The assumed electron and ion collision frequencies are diagrammed in Fig. A.3. In addition, as per Pappert and Moler [1974], a nominal ion mass of 32 amu and a geomagnetic field strength of 0.5 G are used. It is assumed that the propagation path is east to west and that the magnetic field dip is -80 deg. Figures 4 and 5 also show the ambient day and night profiles [Pappert and Moler, 1974].

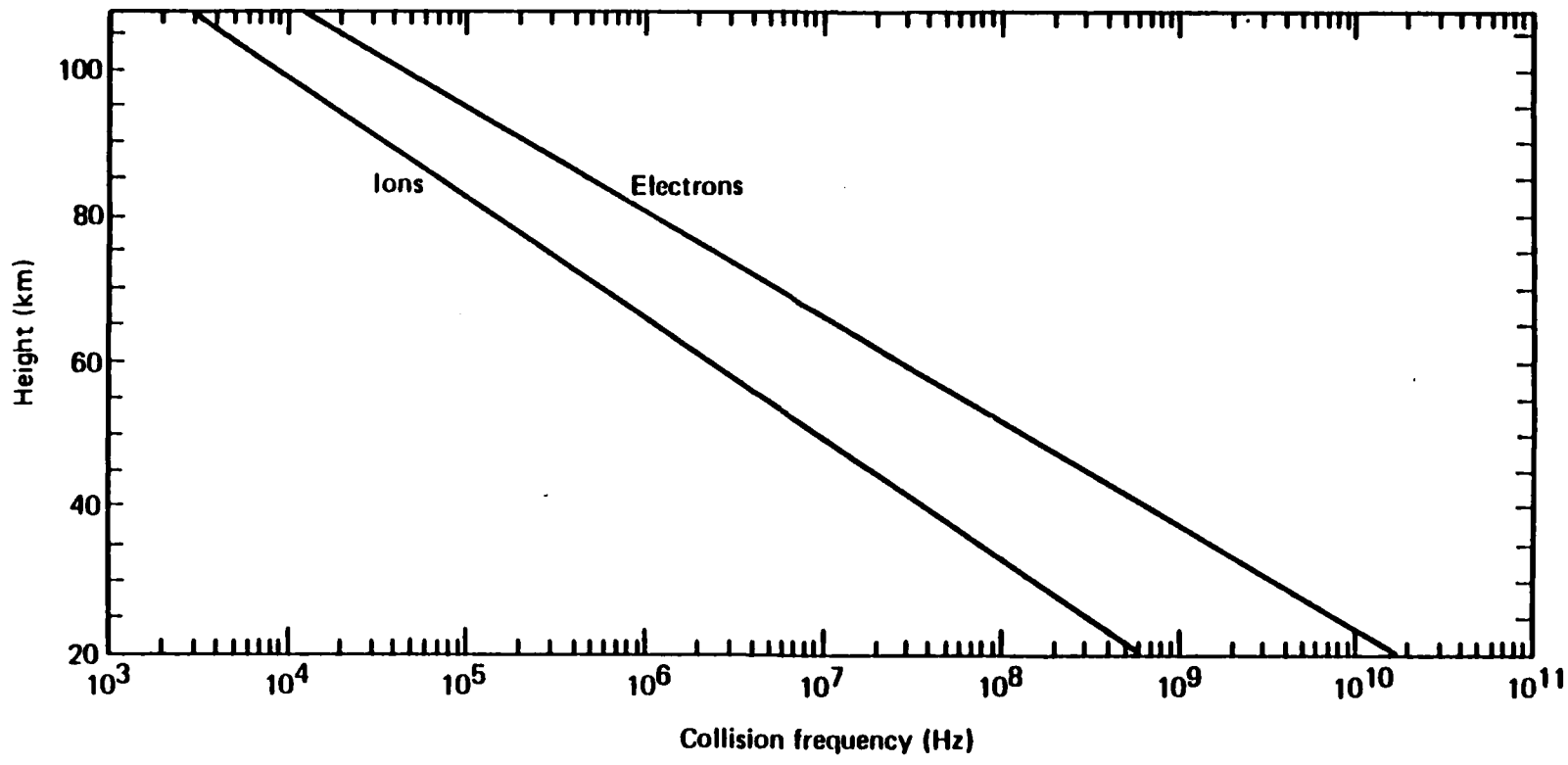

Fig. A.3--Electron and ion collision frequencies

Appendix B

RAY TRACING IN TWO DIMENSIONS

In this appendix we derive the ray-tracing equations (for the two-dimension wave) that solve

$$[\nabla_T^2 + k^2 S^2(x, y)]\ \psi = 0 \ . \tag{B.1}$$

The derivations are based on Budden's [1961b] theory. That theory is presented in full in order to indicate the approximations involved.

Derivation of Ray-Tracing Equations

The propagation constant S is written as follows:

$$S = \mu + i\chi \ .$$

The imaginary part in what follows is neglected, so Eq. (B.1) becomes

$$[\nabla_T^2 + k^2 \mu^2(x, y)]\ \psi = 0 \ . \tag{B.2}$$

Thus μ is equivalent to the refractive index, and it will be referred to as such for convenience.

The solution to Eq. (B.1) can be written as

$$\psi = \psi_0\ e^{-i\varepsilon(x,y)} \ . \tag{B.3}$$

In Eq. (B.3) $\varepsilon(x, y)$ is the eikonal function, which we assume can be written

$$\varepsilon(x, y) = k\left(\int^x P_x\ dx + \int^y P_y\ dy\right) , \tag{B.4}$$

where $P_x(x, y)$, $P_y(x, y)$ are assumed to be proportional to the direction cosines of the two-dimensional field's wave normal, and

$$P_x^2 + P_y^2 = \mu^2 \ . \tag{B.5}$$

In order for ray tracing to be possible it must be assumed that the medium is varying slowly enough so that the spatial derivatives of P_x and P_y are small enough that they can be neglected. (This point will be discussed later.) If that assumption is valid, then

$$P_x = \frac{1}{k}\frac{\partial \varepsilon}{\partial x} \quad \text{and} \quad P_y = \frac{1}{k}\frac{\partial \varepsilon}{\partial y} \ , \tag{B.6}$$

or,

$$\vec{P} = \frac{1}{k}\vec{\nabla}_T \varepsilon \ . \tag{B.7}$$

(The subscript T will hereafter be dropped, because the existence of P_z, which is always zero, is assumed since ε is not a function of z.)

From Eq. (B.7) it follows that:

$$\vec{\nabla} \times \vec{P} = 0 \ ,$$

or,

$$\frac{\partial P_y}{\partial x} = \frac{\partial P_x}{\partial y} \ . \tag{B.8}$$

From Eqs. (B.3) and (B.4) it can be shown that P_x, P_y are proportional to direction cosines of the wave normal at the point x, y. In fact,

$$\frac{P_x}{\left(P_x^2 + P_y^2\right)^{1/2}} \quad \text{and} \quad \frac{P_y}{\left(P_x^2 + P_y^2\right)^{1/2}} ,$$

are the direction cosines of the wave normal. If the wave normal takes all possible directions, then the locus of the point (P_x, P_y) in "refractive index space" defines the refractive index surface G. The equation of this surface may be written

$$G(x, y; P_x, P_y) = \frac{\left(P_x^2 + P_y^2\right)^{1/2}}{\mu(x, y; P_x, P_y)} = 1 , \tag{B.9}$$

where μ is made a function of P_x, P_y to indicate that it may depend on the direction of the wave normal. The ray direction is normal to the refractive index surface, and thus has direction cosines given by

$$\frac{\partial G}{\partial P_x} \quad \text{and} \quad \frac{\partial G}{\partial P_y} .$$

A wavefront is defined as some point in the wave with a particular phase, such as the wave crest. A wavefront travels with the ray velocity V_R. Let x, y be the coordinates at which the wavefront intersects the ray. Hence, $\dot{x}$, $\dot{y}$ are the components of the ray velocity, and must therefore be proportional to $\partial G/\partial P_x$ and $\partial G/\partial P_y$. Budden [1961b] shows that the constant of proportionality is the speed of light c, so

$$\frac{\dot{x}}{c} = \frac{\partial G}{\partial P_x} \quad \text{and} \quad \frac{\dot{y}}{c} = \frac{\partial G}{\partial P_y} . \tag{B.10}$$

Since

$$G(x, y; P_x, P_y) = 1 ,$$

the result must be

$$\frac{dG}{dx} = 0 \quad \text{and} \quad \frac{dG}{dy} = 0 \quad .$$

So, from the left-hand equation above, the following is derived:

$$\frac{\partial G}{\partial x} + \frac{\partial G}{\partial P_x}\frac{\partial P_x}{\partial x} + \frac{\partial G}{\partial P_y}\frac{\partial P_y}{\partial x} = 0 \quad . \tag{B.11}$$

Using Eq. (B.10) yields

$$\frac{\partial G}{\partial x} + \frac{1}{c}\left(\dot{x}\,\frac{\partial P_x}{\partial x} + \dot{y}\,\frac{\partial P_y}{\partial x}\right) = 0 \quad .$$

And doing the same with Eq. (B.8) gives

$$\frac{\partial G}{\partial x} + \frac{1}{c}\left(\dot{x}\,\frac{\partial P_x}{\partial x} + \dot{y}\,\frac{\partial P_x}{\partial y}\right) = 0 \quad ,$$

which can also be written as

$$\frac{\partial G}{\partial x} + \frac{1}{c}\frac{dP_x}{dt} = 0 \quad .$$

Therefore,

$$\dot{P}_x = -\,c\,\frac{\partial G}{\partial x} \quad , \tag{B.12}$$

and

$$\dot{P}_y = -\,c\,\frac{\partial G}{\partial y} \quad . \tag{B.13}$$

Equations (B.10), (B.12), and (B.13) are, taken all together, the canonical equations of the ray.

The variable θ, which is the angle the wave normal makes with the y-axis, is introduced into the calculations as follows:

$$P_x = \mu \sin \theta \quad , \tag{B.14}$$

and

$$P_y = \mu \cos \theta \quad . \tag{B.15}$$

Therefore, using Eqs. (B.12) through (B.15), it can be shown that:

$$\frac{dP_x}{dt} = \frac{d\mu}{dt} \sin \theta + \mu \cos \theta \frac{d\theta}{dt} = - c \frac{\partial G}{\partial x} \quad ,$$

and

$$\frac{dP_y}{dt} = \frac{d\mu}{dt} \cos \theta - \mu \sin \theta \frac{d\theta}{dt} = - c \frac{\partial G}{\partial y} \quad .$$

Solving for $d\theta/dt$ gives

$$\frac{d\theta}{dt} = - \frac{c}{\mu^2} \left[\cos \theta \frac{\partial G}{\partial x} - \sin \theta \frac{\partial G}{\partial y} \right] \quad .$$

Differentiating Eq. (B.9) yields

$$\frac{\partial G}{\partial x} = \frac{\partial}{\partial x} \frac{\left(P_x^2 + P_y^2\right)^{1/2}}{\mu} = - \frac{1}{\mu} \frac{\partial \mu}{\partial x} \quad ,$$

$$\frac{\partial G}{\partial y} = \frac{\partial}{\partial y} \frac{\left(P_x^2 + P_y^2\right)^{1/2}}{\mu} = - \frac{1}{\mu} \frac{\partial \mu}{\partial y} \quad ,$$

and

$$\frac{\partial G}{\partial P_x} = \frac{P_x}{\mu^2} = \frac{\cos\theta}{\mu} \quad ,$$

$$\frac{\partial G}{\partial P_y} = \frac{P_y}{\mu^2} = \frac{\sin\theta}{\mu} \quad .$$

Equations (B.16), (B.17), and (B.18), then, are the ray tracing equations:

$$\frac{d\theta}{dt} = \frac{c}{\mu^2}\left[\cos\theta\,\frac{\partial\mu}{\partial x} - \sin\theta\,\frac{\partial\mu}{\partial y}\right] \quad , \tag{B.16}$$

$$\frac{dx}{dt} = c\,\frac{\sin\theta}{\mu} \quad , \tag{B.17}$$

and,

$$\frac{dy}{dt} = c\,\frac{\cos\theta}{\mu} \quad . \tag{B.18}$$

Validity Criteria

In order to establish the validity of Eq. (B.6) we will consider a situation in which μ is a function of y only (at least locally). In such a situation, P_x cannot depend on x, so it follows that

$$\psi = \psi_0 \exp\left[-ik\left(P_x x + \int^y P_y dy\right)\right] \quad ,$$

which resembles the equation of a field at oblique incidence to the ionosphere.

Just as nS is independent of z in the case of propagation in the ionosphere, it can be shown that P_x is independent of y:

$$\nabla_T^2 \psi = \frac{\partial^2 \psi}{\partial x^2} + \frac{\partial^2 \psi}{\partial y^2}$$

$$= -k^2 \left(P_x^2 + P_y^2 + \frac{i}{k} \frac{\partial P_y}{\partial y} \right) \psi$$

$$= -k^2 \mu^2 \left(1 + \frac{i}{k\mu^2} \frac{\partial P_y}{\partial y} \right) \psi \quad .$$

So, the solution to Eq. (B.2) is valid if

$$\left| \frac{1}{k\mu^2} \frac{\partial P_y}{\partial y} \right| << 1 \quad .$$

By differentiating Eq. (B.5) and using Eq. (B.15) we obtain

$$\frac{\partial P_y}{\partial y} = \frac{1}{\cos \theta} \frac{\partial \mu}{\partial y} \quad .$$

Therefore, the following is the validity criterion:

$$\left| \frac{1}{k\mu^2 \cos \theta} \frac{\partial \mu}{\partial y} \right| << 1 \quad . \qquad \text{(B.19)}$$

This will fail for any value of $\frac{\partial \mu}{\partial y}$ or μ if θ is near 90 deg.

Typically $\Delta\mu \cong 0.1$, $\Delta y \cong 1$ Mm, $\mu \cong 1.20$, and $k = 1.57$ 1/Mm at 76 Hz. Thus, at $\theta = 0$, if we say $\partial\mu/\partial y \approx \Delta\mu/\Delta y$, then,

$$\frac{1}{k\mu^2} \frac{\partial \mu}{\partial y} = 0.044 \quad .$$

Therefore, for an accurate ray trace,

$$0.044 \ll \cos\theta \quad ,$$

or,

$$\theta \ll 87 \text{ deg} \quad .$$

To obtain a more precise understanding, 0.1 is taken as the upper limit on the left-hand side of Eq. (B.19). This yields

$$\frac{0.044}{\cos\theta} < 0.1 \quad ,$$

or,

$$\cos\theta > 0.44 \quad .$$

Therefore, rays that make angles with the y-axis of $\theta < 65$ deg are valid. If 0.2 is the upper limit, then rays with $\theta < 77$ deg are valid.

In the above, μ was assumed to change only in the y-direction. In fact, the disturbance of 23 November 1982 is a function of the distance from the north pole. However, Eq. (B.3) must be a solution at each point in space. Therefore if the y-axis is taken locally to be along the gradient of μ, then Eq. (B.19) should yield the local validity condition, which is expected to fail at right angles to the direction of $\vec{\nabla}\mu$. The validity condition can be written as

$$\left|\frac{1}{\cos\theta}\,\frac{1}{\mu^2}\,\frac{d\mu}{dr}\right| \ll 1 \quad . \tag{B.20}$$

In the above calculations, $\partial\mu/\partial r$ is approximated by $\Delta\mu/\Delta r$. However, using Eq. (4) gives the value of $\partial\mu/\partial r$ at all points. Since no absorption is assumed in Sec. V, S can be substituted for μ. Then, letting $\Delta S = S_{SPE} - S_{AMB}$, Eq. (4) can be written

$$S(r) = -\frac{\Delta S}{2}\left\{\frac{1 - \exp\left[-\frac{(r - r_0)}{\delta r}\right]}{1 + \exp\left[-\frac{(r - r_0)}{\delta r}\right]}\right\} + S_{AMB} + \frac{\Delta S}{2} \quad ,$$

The inner and outer radii of the boundary region, r_1 and r_2, respectively, [as shown in Fig. 7 on p. 17 and defined by Eqs. (5) and (6) on p. 17] can be expressed by the relations

$$S(r_1) = +\frac{\Delta S}{2}\,0.95 + S_{AMB} + \frac{\Delta S}{2} \quad ,$$

and

$$S(r_2) = -\frac{\Delta S}{2}\,0.95 + S_{AMB} + \frac{\Delta S}{2} \quad .$$

Solving for r_1 and r_2 yields

$$\frac{(r_1 - r_0)}{\delta r} = 3.66 \quad ,$$

and

$$\frac{(r_2 - r_0)}{\delta r} = -3.66 \quad ,$$

or,

$$(r_2 - r_1) = 7.33\ \delta r \quad .$$

Therefore,

$$\delta r = \frac{\Delta r}{7.33} \quad . \tag{B.21}$$

The derivative of S becomes

$$\frac{dS}{dr} = -\frac{\Delta S}{2} \frac{2}{\left\{1 + \exp\left[-\frac{(r - r_0)}{\delta r}\right]\right\}^2} \frac{1}{\delta r} \exp\left[-\frac{(r - r_0)}{\delta r}\right] \quad . \tag{B.22}$$

This derivative has a maximum at $r = r_0$, so the maximum is

$$\frac{dS}{dr} = -\frac{\Delta S}{4} \frac{1}{\delta r} = -\frac{7.33}{4} \frac{\Delta S}{\Delta r} = 1.8 \frac{\Delta S}{\Delta r} \quad . \tag{B.23}$$

The left-hand side of Eq. (B.20) can now be calculated for the following three situations discussed in Sec. V: (1) the weak SPE with a 1 Mm transition zone, (2) the strong SPE with a 1 Mm transition zone, and (3) the weak SPE with a 0.5 Mm transition zone. Table B.1 gives the results.

The values in Table B.1 were calculated for the maximum value of the derivative. The validity condition is improved considerably at distances nearer to or farther from the north pole than r_0. This is illustrated by the plot in Fig. B.1, which shows the validity criterion for situation 3 at 80 deg as a function of distance from the north pole.

Table B.1

Validity Criterion For Three Examples

Angle with Respect to Gradient (deg)	Example 1 $S_{SPE} = 1.25$ $\Delta S \cong 0.1$ $\Delta r \cong 1$ Mm	Example 2 $S_{SPE} = 1.45$ $\Delta S \cong 0.3$ $\Delta r \cong 1$ Mm	Example 3 $S_{SPE} = 1.25$ $\Delta S \cong 0.1$ $\Delta r \cong 0.5$ Mm
0	0.081	0.207	0.162
60	0.162	0.414	0.324
65	0.191	0.489	0.383
70	0.237	0.605	0.473
75	0.313	0.799	0.625
80	0.466	1.191	0.932
85	0.928	2.373	1.857

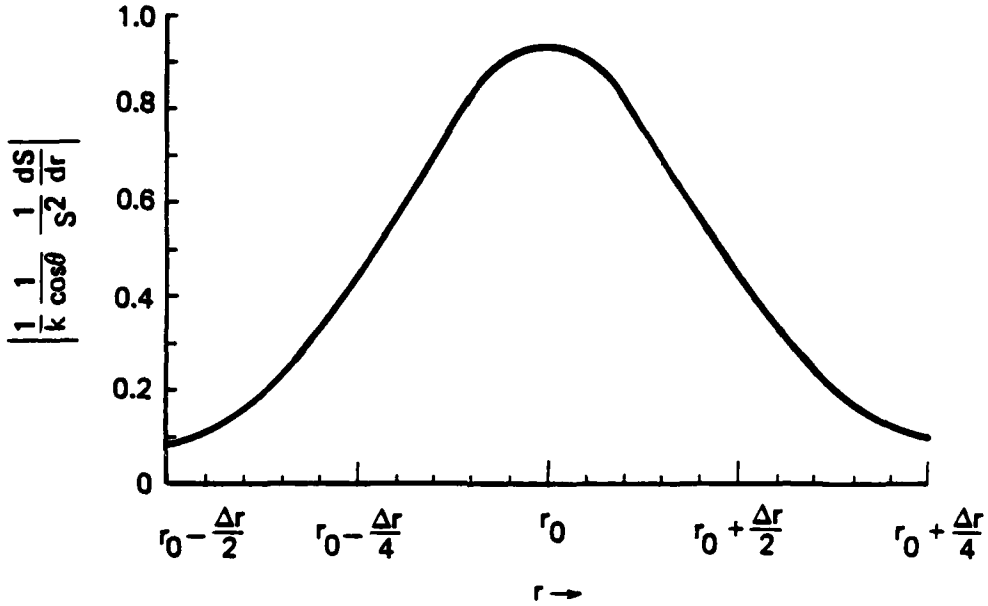

Fig. B.1--Validity condition for $S_{SPE} = 1.25$

REFERENCES

Bannister, P. R., "Localized ELF Nocturnal Propagation Anomalies," Radio Sci., Vol. 17, No. 3, May-June 1982, pp. 627-634.

Budden, K. G., Radio Waves in the Ionosphere, Cambridge University Press, New York City, 1961a.

-----, The Waveguide Mode Theory of Wave Propagation, Logos, London, 1961b.

Field, E. C., "The Effects of Ions on Very Low Frequency Propagation during Polar Cap Absorption Events," Radio Sci., Vol. 5, No. 2, 1970, pp. 591-600.

Field, E. C., and R. G. Joiner, "Effects of Lateral Ionospheric Gradients on ELF Propagation," Radio Sci., Vol. 17, May-June 1982, pp. 693-700.

-----, "An Integral-Equation Approach to Long-Wave Propagation in a Nonstratified Earth-Ionosphere Waveguide," Radio Sci., Vol. 14, November-December 1979, pp. 1057-1068.

Galejs, J. Terrestrial Propagation of Long Electromagnetic Waves, Pergamon Press, New York City, 1972.

Greifinger, C., and P. Greifinger, "Approximate Method for Determining ELF Eigenvalues in the Earth-Ionosphere Waveguide," Radio Sci., Vol. 13, No. 5, 1978, pp. 831-837.

Katan, J. R., and P. R. Bannister, "Observation of ELF Propagation Variations at Mid and High Latitudes during the November/December 1982 Solar Proton Events," Naval Underwater Systems Center, New London, Connecticut, Technical Report, forthcoming.

Knapp, W. S., and K. Schwartz, Aids for the Study of Electromagnetic Blackout, Defense Nuclear Agency, Washington, D.C., DNA 3449, 1 February 1975 (submitted by General Electric/TEMPO).

Pappert, R. A., "Effects of a Large Patch of Sporadic-E on Night-Time Propagation at Lower ELF," J. Atmos. Terr. Phys., Vol. 42, 1980, pp. 417-425.

Pappert, R. A., and W. F. Moler, "Propagation Theory and Calculations at Lower Extremely Low Frequencies (ELF)," IEEE Trans. Commun., Vol. COM-22, No. 4, 1974, pp. 438-451.

Reid, G. C., "Polar Cap Absorption--Observations and Theory," in C. Gordon, V. Canuto, and I. Axford (eds.), The Earth: 1. The Upper Atmosphere, Ionosphere and Magnetosphere, Gordon and Breach, New York City, 1978, pp. 269-302.

Sauer, H., private communication, National Oceanic and Atmospheric Administration, Boulder, Colorado, April 1983.

Wait, J. R., Electromagnetic Waves in Stratified Media, Pergamon Press, New York City, 1970.

END

FILMED

12-85

DTIC